



UPPSALA
UNIVERSITET

*Digital Comprehensive Summaries of Uppsala Dissertations
from the Faculty of Science and Technology 2097*

Liquid metal microscale deposition for soft and stretchable skin-like electronics

Providing a soft and gentle contact to living beings

BEI WANG



ACTA
UNIVERSITATIS
UPSALIENSIS
UPPSALA
2021

ISSN 1651-6214
ISBN 978-91-513-1349-8
URN urn:nbn:se:uu:diva-459339

Dissertation presented at Uppsala University to be publicly examined in Polhemsalen, Lägerhyddsvägen 1 752 37, Uppsala, Wednesday, 19 January 2022 at 09:00 for the degree of Doctor of Philosophy. The examination will be conducted in English. Faculty examiner: Professor Magnus Berggren.

Abstract

Wang, B. 2021. Liquid metal microscale deposition for soft and stretchable skin-like electronics. Providing a soft and gentle contact to living beings. *Digital Comprehensive Summaries of Uppsala Dissertations from the Faculty of Science and Technology* 2097. 74 pp. Uppsala: Acta Universitatis Upsaliensis. ISBN 978-91-513-1349-8.

Skin-like electronics could provide a soft and gentle contact with living beings for perceiving and delivering the information of pressure, strain, temperature with higher spatial resolution and sensitivity than our skin, without disturbing the user. Gallium-based liquid metal (LM) is an excellent material for soft and stretchable skin-like devices, since it has high electrical and thermal conductivity, flowability, and self-healable capability. However, the LM patterning technique is not well developed and has challenges due to its high surface tension. This thesis presents several methods to advance LM patterning capability, targeting thin, homogenous, high-resolution, and high-density skin-like electronics. Especially, masked deposition is a versatile technique in microsystem fabrication but has been limited by the masking and deposition. Firstly, a mask material that is well suited for lift-off processing at high resolution has been sought for. In this thesis, we introduced the use of a water dissolvable sacrificial thin polyvinyl alcohol (PVA) film for LM masked deposition. The dyed PVA film could be cut by laser and the fabricated mask had a resolution down to 20 μm in width. Secondly, our previously demonstrated LM atomization has a large variation of the droplets size generated by the airbrush, which severely hinder the depositing uniformity at microscale. Sonication produced LM particles has a narrow size distribution, but the particles are insulating. We proposed a simple and effective technique to merge these particles by precise spraying, depositing a LM layer that is microscale thin (5 μm), smooth (area roughness, $S_a=0.8 \mu\text{m}$), and gas permeable. More importantly, it has conductivity similar to pure LM. With this technique, a skin-like high resolution sensor was fabricated, which is able to monitor the local wrinkle skin movement. Moreover, a high-resolution skin-like micro-heater was made and placed on the fragile and oval abdomen of *Drosophila* for localized ectopic genetic expression in its gut. In addition, printing LM based skin-like electronics on a 3D surface is also challenging. Hence, we developed two complementary techniques that could gently and conformally transfer a planar pattern to a 3-D surface: A PDMS-based flexible stamp that could transfer a 2-D pattern to a 3-D surface and hydro printing with PVA film as a medium. Using hydro printing, the circuit that was transferred on delicate plants could monitor their physiological information and control their growth.

Keywords: laser patterning, sacrificial mask, liquid metal, strain sensor, skin movement, masking, shrink film, 3D conformal masking, liquid metal particles, soft electronics, stretchable electronics, compliant electronics, skin-like electronics, epidermal electronics, micro-heater, particle sintering, enteroendocrine cells, localized ectopic expression, wettability, flexography printing, conformal transfer printing, hydro printing, plant physiology, *drosophila*

Bei Wang, Department of Materials Science and Engineering, Microsystems Technology, Box 35, Uppsala University, SE-751 03 Uppsala, Sweden.

© Bei Wang 2021

ISSN 1651-6214

ISBN 978-91-513-1349-8

URN urn:nbn:se:uu:diva-459339 (<http://urn.kb.se/resolve?urn=urn:nbn:se:uu:diva-459339>)

做一个有用趣的人，做一个有用的人。

Be a humorous person, be a wise person.

Svensk Sammanfattning

Människohud är ett komplext system. Det skyddar vår kropp från omgivningen och gör att vi kan uppfatta olika omgivande objekts signaler, såsom temperatur, tryck, textur och form. Det finns olika högspecialiserade sinnesreceptorer i vår hud som kan upptäcka signalen och låta oss veta den omgivande situationen.

Inspirerad av detta mänskliga organ kan den konstgjorda hudliknande elektroniken ge ökad prestanda till sensorer, både i överlägsen rumslig upplösning och känslighet. Dessutom skulle elektroniken kunna ges ytterligare funktioner som kemisk och biologisk avkänning, mäta egenskaper som biologisk nedbrytbarhet och att den får tillräckligt med energi från omgivningen för att inte behövas laddas upp med en batteriladdare.

På 1970-talet inspirerade science fiction tanken om konstgjord hud. Före 2000 var den gjord av flexibla men inte töjbara material. Forskare integrerade stora, lågkostnads- och utskrivbara sensorer på flexibla material för att efterlikna hudfunktionen. Efter det började töjbar elektronik, såsom töjbara OLED:er, batterier och kretsar, dyka upp. 2011 föreslog Rogers grupp en töjbar epidermal hudliknande elektronik som integrerade antenn, töjningsmätare, temperatur, RF-spole, och en EKG/EMG-sensor. Denna elektronik är tunn, flexibel och töjbar, klabbig mot huden och kan röra sig synkront med huden, vilket är en milstolpe för hudliknande elektronik. Fram till nu har forskare arbetat med det från material, bearbetningstekniker, funktionella komponenter för att föra det närmare vår ursprungliga dröm.

Det finns några typiska egenskaper hos hudliknande elektronik. För det första måste den vara tunn, flexibel och töjbar, det vill säga ha liknande fysiska egenskaper som vår hud. Så när den arbetar på vår hud, som en del i bärbara mjuka robotmaterial eller proteser, kan den röra sig synkront och minimera fel och att den stör så mycket som möjligt. Dessutom bör den vara självhäftande till målytan för att underlätta direkt montering. Andra egenskaper bör också övervägas, som att vara biologiskt kompatibel med vår hud, som t.ex. släppa igenom gas för att undvika att generera inflammatoriska problem, och helst även vara biologiskt nedbrytbar efter användning.

Ännu viktigare är att den kan ge taktil avkänning, för att uppfatta tryck, belastning, glid och textur, och temperatur. Förutom känsselförmågan hos vår hud, kommer det att vara intressant att införliva funktioner som stödjer hälso-

övervakning och avkänning av kroppsrörelser. Denna utveckling kräver studier av många områden, inklusive material, kretsar, sensorer, energilagring och -skördning, modellering, masstillverkning, kringutrustning, och digital kommunikation.

I denna doktorsavhandling studeras mönstrad deponering och transfertryckning för att mönstra galliumlegeringar som är flytande i rumstemperatur (jag kallar dem vätskemetaller från engelskans liquid metals), med inriktning på att tillverka vätskemetallbaserad hudliknande mjuk, tunn och högupplöst elektronik. Det kan ge en mjuk och skonsam kontakt till levande varelser för att upptäcka och stimulera information.

Mönstrad deponering där en mask skyddar större delen av ytan och öppningar i den tillåter att ett mönster deponeras är en av de mest lovande teknikerna för skalbar vätskemetallbaserad töjbar elektroniktillverkning. Vi fokuserade på två kritiska aspekter av denna teknik, som är masktillverkning och vätskemetalldeponering. Vad det gäller masktillverkningen har vi tagit fram två nya masker: En PVA-mask som kan lösas upp i vatten är ett oskiljaktigt element när mönstringsupplösningen når en hög nivå. Dessutom har vi tagit fram en krympmask som kan dra ihop sig till en fjärdedel av sin ursprungliga dimension, vilket ger möjlighet att använda vanliga lågkostnadsutrustningar i maskframtagningen. Vad det gäller vätskemetall-deponeringen har vi tagit fram ytterst små (i storleksordningen av en bakterie, dvs mikrometer/submikrometer-stora där en mikrometer är en tusendels millimeter) vätskemetallpartiklarna som kan deponeras med ett gott utbyte till en upplösning av 25 mikrometer.

Arbetet med PVA-masken som kan upplösas i vatten innehåller en hel del bearbetningsteknik för att mönstra komplexa och kompakta vätskemetallmönster på tunna sträckbara substrat, inklusive PVA-filmberedning, masktillverkning, överföring, vätskemetallavsättning och utveckling, komponenterintegration och inkapsling. I varje steg diskuterades och analyserades de tekniska frågorna. Det involverar PVA-modifiering, laserablation, adhesionsjustering, engångsöverföringsmetodik, etc. Med denna nya teknik tillverkades epidermala trådtöjningsgivare med vätskemetallmönster i hög täthet och upplösning. Givarna fästes sedan på ett finger för att övervaka fina lokala hudrörelser som hur rynkor som bildas ändras när fingerlederna böjs.

När det gäller krympmask föreslog vi en maskeringsteknik baserad på en krympfilm som kan göra högupplösta masker med hjälp av en mekanisk skärplotter (som normalt används för att skära vinyltejp till reklamtexter) tillsammans med en vanlig ugn. Efter krympning kan krympmaskmönstrets bredd och utrymme minska till ungefär en tredjedel av det ursprungliga skurna mönstret med potential att nå ännu längre. Dessutom visade vi att masken kunde läggas inte bara på plana ytor utan även på cylindrar eller sfärer.

Arbetet med deponering föreslog ett sätt att använda kollisionssorsakade brott för sintring av mikrometer/submikrometer-små vätskemetallpartiklar. Att få

dessas partiklar att förenas till en kropp utan ingrepp är nästan omöjligt på grund av deras viskoelastiska skal och inre vätska med hög ytspänning. Sammansmältningen kan dock bli verklighet genom att kollidera med vätskemetallpartiklars kärn-skal-strukturer med tillräckligt hög kraft så att skalet spricker. Med denna teknik tillverkades en följsam hudliknande mikrovärmare med hög täthet och upplösning för att termiskt aktivera lokala gen uttryck hos celler i buken av en bananfluga, vilket kan ge bättre medicinska studier med genmodifierade bananflugor.

Flexografityck används ofta i tryckerier. Genom att justera vätskemetallens vätbarhet till en yta genom att göra de ytor som inte ska väta väldigt ojämna (på mikrometer-nivå), presenterade denna avhandling en flexografityckteknik för att överföra mönster flytande legeringskretsar på både plana och 3D-komplexa ytor, och har även undersökt hur man optimerar tryckningen och sambandet mellan vätbarheten och hur ytans ruffhet ändras.

PVA-film kan också vara ett medium för att överföra vätskemetallmönstret från en 2D-yta till en 3D-yta. En skonsam tryckteknik där man lägger PVA-filmen på en vattenyta för att kunna mönstra elektronisk på växter togs fram. På så sätt kan elektroniken känna av fysiologiska signaler och till och med fungera som en biohybrid för att styra växtbeteendet. Elektroniken kunde övervaka bladfuktighet och längd, och manipulera blad- och böngroddarorienteringen.

Sammanfattningsvis har vi utforskat vätskemetallmönstertekniker och med hjälp av dem tillverkat flera vätskemetallbaserade hudliknande elektronikkomponenter. Funktionerna som att känna av hudrörelser, termisk aktivering, och växttillväxtövervakning demonstrerades, vilket indikerar att våra föreslagna tekniker är bra lösningar på utmaningen med hudliknande elektronik.

List of Papers

This thesis is based on the following papers, which are referred to in the text by their Roman numerals.

- I **Bei Wang**, Kang Wu, Klas Hjort, Chuanfei Guo, Zhigang Wu. High-Performance Liquid Alloy Patterning of Epidermal Strain Sensors for Local Fine Skin Movement Monitoring. *Soft Robotics* 2019, 6, 414.
- II **Bei Wang**, Wenci Xin, Klas Hjort, Chuanfei Guo, Zhigang Wu. Sandwiched Polyethylene Shrink Film Masking with Tunable Resolution and Shape for Liquid Alloy Patterning, *ACS Appl. Polym. Mater.* 2019, 1, 145–151.
- III **Bei Wang**, Junjun Gao, Jiajun Jiang, Zenghui Hu, Klas Hjort, Zheng Guo, Zhigang Wu. Liquid metal microscale deposition enabled high-resolution microheater for localized ectopic expression in *Drosophila*. *Adv. Mater. Technol.* 2021, 2100903
- IV Shuo Zhang, **Bei Wang**, Jiajun Jiang, Kang Wu, Chuan Fei Guo, Zhigang Wu. High Fidelity Conformal Printing of 3D Liquid Alloy Circuits for Soft Electronics. *ACS Appl. Mater. Interfaces* 2019, 11, 7148.
- V Jiajun Jiang, Shuo Zhang, **Bei Wang**, Han Ding, Zhigang Wu. Hydroprinted Liquid-Alloy-Based Morphing Electronics for Fast-Growing/Tender Plants: From Physiology Monitoring to Habit Manipulation. *Small* 2020, 2003833.

Reprints were made with permission from the respective publishers.

Author's contribution

- I Most of planning, designing, experiment, characterization, analysis, and the majority of discussion and writing.
- II Most of planning, designing, experiment, characterization, analysis, and the majority of discussion and writing.
- III Most of planning, designing, experiment, characterization, analysis, and the majority of discussion and writing.
- IV Major part of planning, designing, experiment, characterization, analysis, discussion and writing.
- V Part of planning, designing, experiment, characterization, analysis and major part of discussion and writing.

Contents

1. Introduction.....	15
1.1 Soft and stretchable electronics.....	15
1.2 Liquid metal based stretchable electronics.....	16
1.3 Liquid metal patterning	17
1.3.1 Patterning with bulk liquid metal	18
1.3.2 Patterning with particles	21
1.4 Scope of the thesis.....	23
2. Materials and processing techniques.....	26
2.1 Materials.....	26
2.1.1 Liquid metal.....	26
2.1.3 Silicones.....	28
2.1.4 Shrink film.....	29
2.2 Mask fabrication.....	29
2.2.1 Sacrificial PVA mask	29
2.2.2 Shrink film mask.....	30
2.3 Lift-off patterning.....	34
2.3.1 The processing technique	34
2.3.2 Performance characterization	36
2.4 Deposition with liquid metal particles.....	38
2.4.1 Liquid metal particles	38
2.4.2 LM micron/submicron particles merging	41
2.4.3 Comparison of LM deposition methods	45
2.4.4 Microscale deposition based lift-off patterning	47
2.5 Transfer printing techniques.....	49
2.5.1 Stamp printing	49
2.5.2 Hydroprinting	50
3 Applying a conformal and gentle contact to living beings	52
3.1 Epidermal Strain Sensor.....	52
3.2 Compliant micro-heater.....	55
3.3 Plants monitoring and manipulation.....	58
4. Summary of papers	60
Paper I. High-Performance Liquid Alloy Patterning of Epidermal Strain Sensors for Local Fine Skin Movement Monitoring	60

Paper II. Sandwiched Polyethylene Shrink Film Masking with Tunable Resolution and Shape for Liquid Alloy Patterning	61
Paper III. Liquid metal microscale deposition enabled high resolution and density epidermal microheater for localized ectopic expression in <i>Drosophila</i>	62
Paper IV. High Fidelity Conformal Printing of 3D Liquid Alloy Circuits for Soft Electronics.....	63
Paper V. Hydroprinted Liquid-Alloy-Based Morphing Electronics for Fast-Growing/Tender Plants: From Physiology Monitoring to Habit Manipulation	64
4. Conclusion	65
5. Acknowledgements.....	67
Reference	69

Abbreviations

CA	Contact Angle
CNT	Carbon Nanotube
cPDMS	Carbon-doped PDMS
DP	Degree of Polymerization
ECG	Electrocardiogram
ee	Enteroendocrine
GFP	Green Fluorescence Protein
IPA	Isopropyl Alcohol
LM	Liquid Metal
PDMS	Polydimethylsiloxane
PE	Polyethylene
PET	Polyethylene Terephthalate
PPG	Photoplethysmogram
PVA	Polyvinyl Alcohol
SAM	Self-assembled monolayer
SEBS	Styrene-ethylene-butylene-styrene
SEM	Scanning electron microscope
TEM	Transmission Electron Microscopy
UV	Ultraviolet
XCT	X-Ray computed tomogram

1. Introduction

1.1 Soft and stretchable electronics

Today, there is a rapid development of wireless smart devices for sports, fitness, and healthcare: Smart watch that detect blood pressure change in the vascular of patients are in daily use. By measuring electrophysiological signals with several electrodes, the obesity and fat level can be determined [1]. Electrodes attached to the chest can diagnose a person's cardiac disease. These flexible systems can be integrated into a central system to monitor human health state in real time.

However, these products are not enough to collect the user's full information. Imagine that a mother can see the baby's heartbeat on a film attached to her skin [2] by wearing an electronics with biometric sensors. With wireless transmission, the father can experience the same vibrations by a haptic actuator. Imaging even further, parents may feel children's physical or emotional reactions through an electronics skin worn on kids, even they are in distance. This feeling, in turn, can provide essential information to improve and regulate the growth strategy of their kids. Moreover, they cannot only be adapted to interface with human beings, but they are also suitable for insects, animals, and plants. Pets like cats and dogs are important friends and family members to many people, but they can't express their illness symptoms by language. For botany research, it is interesting to monitor physiological signals of growing plants in real-time.

Flexible and stretchable epidermal electronics [3-6], which can compliantly attach to human skin, could collect its receptor's initial and full information. Scientists have advanced these perceiving and sensing systems further to detect information from soft and stretchable objects by mimicking the function of the skin. The skin-like electronics are capable of detecting pressure, temperature, texture, and shape, and they can perceive this information with higher spatial resolution and sensitivity. Moreover, they could detect additional information like strain, chemical, and biological signals, with extra features like biodegradability and self-powering.

Soft and stretchable skin-like electronics with a series of embedded sensors could record the throat vibration of a singer to mimic the rhythm of music [7-9], measure an athlete's movement for rigorous exercises [10], and monitor the patient's neck and other joint motions [11-15]. Rogers's group recently

developed a patch targeting continuous monitoring vital signs for neonatal intensive care, a bimodal, wireless epidermal electronic system [16], Figure 1a. A stretchable human-machine interface that has a four-layer design, eight-channel sensing, and Bluetooth data communication was also developed [17], Figure 1b. As a complete stretchable system, it has sensors, processors, communication module, antennas, *etc.* So far, the development of stretchable semiconductors for functional processors has started [18, 19], some stretchable active components are suggested to be used in the near future, Figure 1c.

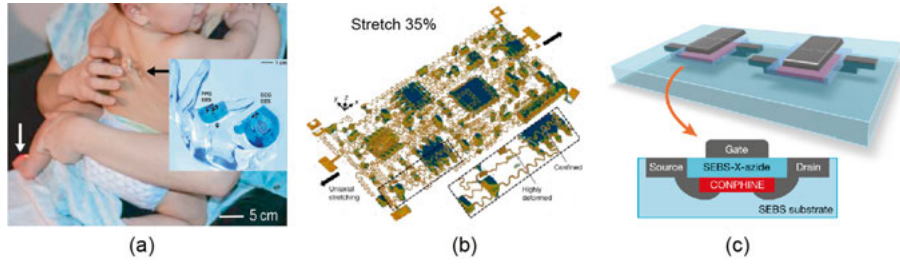


Figure 1. Stretchable electronics. (a) An infant with a PPG device on the foot and an ECG device on the back. Images of devices draped over the fingers of a life-sized, transparent mannequin hand. (Reproduced with permission from ref. [16]) (b) XCT images of the system. (Reproduced with permission from ref. [17]) (c) Example of an intrinsically stretchable transistor array. (Reproduced with permission from ref. [19])

To enable future applications with skin-like electronics, many challenges in manufacturing should be solved. In addition, to enable such functional systems, even more aspects should also be considered [20-22], including materials, circuits, sensors, energy storage and harvesting, modelling, mass fabrication, peripherals, digital communication. To conclude, skin-like electronics have high potential but still need much development before it will be commonly used in society. This thesis is one step towards this future.

1.2 Liquid metal based stretchable electronics

Soft and stretchable skin-like electronics build bridges to extend the communication system to soft and stretchable objects. It is thin, stretchable, and sticky so it can adhere to the carrier and move and stretch synchronously without taking noticeable side effects. Elastomers, such as polydimethylsiloxane (PDMS) and styrene-ethylene-butylene-styrene (SEBS) have a low Young's Modulus that is similar to skin, and are easily processed into thin dielectric layers.

For stretchable conductors, there are three strategies (Figure 2), solid yet thin wavy or meandering metal [16-17], composites conductive additives (particles, flakes and fibres) in polymer [11-13, 23-25], intrinsically stretchable materials

[21, 26-35]. Usually, the wavy metal can't have a high stretchability and has fatigue issues when conducting rigid components. The conductivity of composites is not stable during the stretching. Among these, liquid metal or alloy has high potential because of its high electrical and thermal conductivity and intrinsic infinite stretchability. Moreover, its self-healing property, which means its conductivity can recover after damaging, make it distinctive among sorts of stretchable conductors.[35] Thus, LM is an attractive material in soft and stretchable devices for either functional components or stretchable connectors. Several functional components have been published recently (Figure 2), for example, antennas [26-27], tunnel junctions [28], memristors [29], energy harvesting [30-31], micro-pump [32-33], and sensors [34].

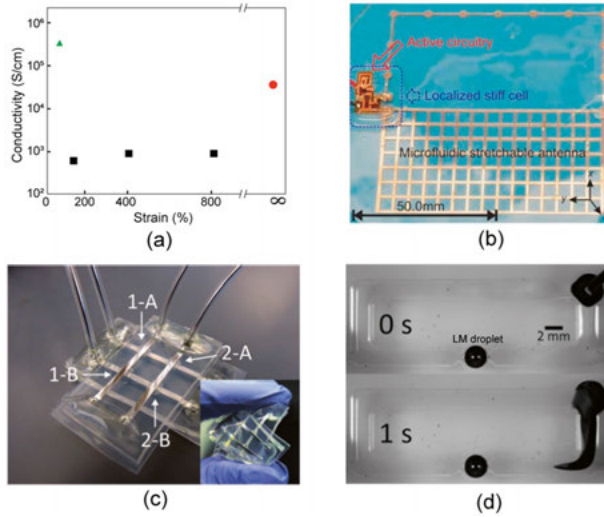


Figure 2. Stretchable conductors and liquid metal based functional components. (a) Comparison of typical conductors for thin stretchable electronics (triangle, square and circle indicate thin wavy metal, composites and LM, respectively. All data extracts from ref. [21]). (b) Stretchable RF radiation sensor. (Reproduced with permission from ref. [27]) (c) An integrated soft memristor circuit. (Reproduced with permission from ref. [29]) (d) LM droplet-based pump. (Reproduced with permission from ref. [33])

1.3 Liquid metal patterning

Due to the high surface tension, low viscosity, and spontaneous oxide shell, it is challenging to fabricate thin, uniform LM patterns at high resolution and complexity. LM patterning basically contains two processes, separating LM from the bulk and fixing it to the target object. Due to the high surface tension and the liquid property, separating LM from the bulk in reservoir, such as the separations happened at the nozzle of direct writing technique or at the orifice

of spraying atomization, could bring instability and limit the patterning capability.

On the other hand, due to the strong metallic bonding of metal atoms, the difference of surface energy is enormous compared to the surface energy of polymer materials, which is dominated by intermolecular bonding. There are two strategies commonly used to bridge this difference, either by utilizing its natural oxide layer or by introducing high-energy materials. The natural oxide layer of LM is reported to be very sticky to many materials. The adhesion provided by this oxide layer can bridge the large surface energy difference, fixing the patterned LM to the elastomer substrate. For example, direct writing, imprinting, and masked deposition take advantage of this sticky layer to stabilize the pattern. Another commonly used strategy is that by coating a transitional nanoscale layer of high-surface energy materials, such as gold, copper, nickel, or chromium, on the target substrate, which have good wettability with LM.

In recent years, researchers have developed many patterning techniques. In this thesis, the processing techniques are divided into two groups, additive and subtractive manufacturing. In additive manufacturing, LM patterns are printed directly on the target substrate, such as direct writing, inkjet printing, 3D-printing, and injection. In subtractive manufacturing, the LM pattern is formed by selectively removing part of the preformed LM layer, such as masked printing, imprinting, and laser cutting.

1.3.1 Patterning with bulk liquid metal

In additive manufacturing, when there is a sufficient adhesion, LM are printed directly on the target substrate[36-39]. As shown in Figure 3a, in direct printing the LM is first extruded from the nozzle, adhered onto the substrate, and patterned by the head's movements in x-y coordination plane. The cross-section of the pattern can be adjusted by the moving speed of the head, the LM flow rate, the needle distance to the substrate, and the substrate's properties. With proper parameters, the line width can reach below 100 μm .

As an alternative to extrusion, inkjet printing has been developed (Figure 3b). Because of the Rayleigh instability, the LM stream breaks into droplets after leaving the needle at high speed. The reported smallest LM droplet was about 10 μm with a flow rate of 0.8 mL/min. The resolution was approximately 100 μm in width, balancing the inkjet speed and the head moving velocity [40, 41].

Injection is a handicraft technique to fabricate components with low pattern complexity, like antennas, by filling pre-fabricated microchannels with LM (Figure 3c). The microchannel usually is made by common molding techniques, which have various formats and designs. However, since all channels

must be connected, the pattern format is limited. Although LM has low viscosity, its surface tension makes the injection process difficult, especially when the substrate is a soft material and has a thin thickness. The reported narrowest line can be down to tens of microns, but the whole pattern is limited due to the replicating and moulding process [26, 34, 42-46].

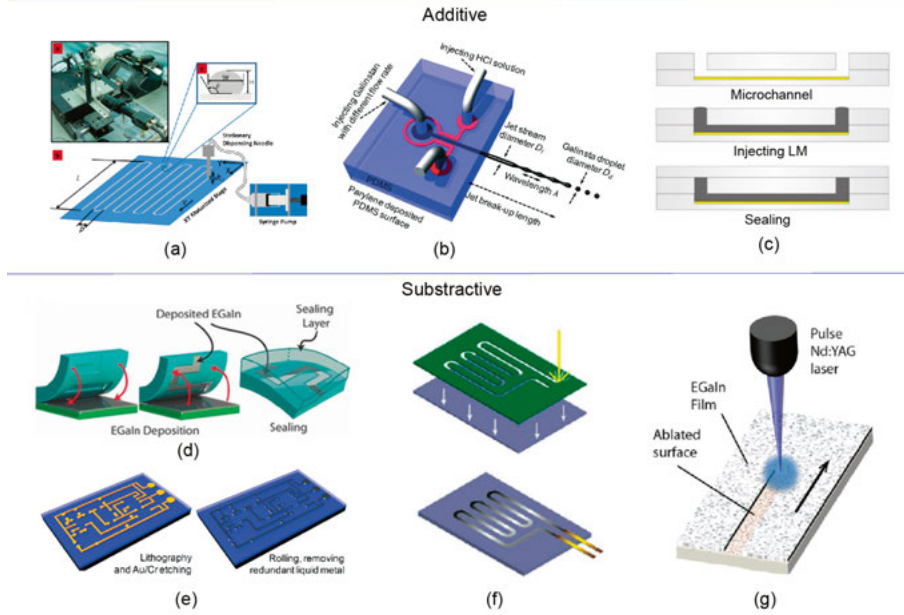


Figure 3. Patterning techniques based on separating from bulk LM. (a) Direct writing [36] (Reproduced with permission from ref. [36]), (b) inkjet printing (Reproduced with permission from ref. [40]), (c) injection (Reproduced with permission from ref. [43]), (d) imprinting (Reproduced with permission from ref. [47]), (e) selective wetting (Reproduced with permission from ref. [49]), (f) masked deposition (Reproduced with permission from ref. [52]) and (g) laser ablation (Reproduced with permission from ref. [58]).

The subtractive fabrication indicates a group of techniques that selectively remove metal from the LM films, such as imprinting, selective wetting, mask deposition, and laser ablation.

Imprinting removes the residual LM from bulk donor LM film by the applied pressure. The open channel's sharp corner acts as a knife to separate the LM during the lift-off process. Since the firm adhesion of oxide skin, the LM can remain inside the channel to form the conductive pattern after separating [47].

With a copper pattern produced by standard photolithography and etching, the LM can attach and remain on it to form a pattern after removing residual LM. The copper has high surface energy, which makes its super high wettability to

LM, and this can bind a small amount of LM and separate it from bulk LM film during lift-off [48-49].

With a stencil mask, only the LM that passes through the mask openings can deposit on the target substrate. The process of separation of LM is critical, especially when the resolution is up to the microscale. In this case, when the bulk LM particle hits or squeezes the open channel's sharp corner, the bulk LM droplet is cut into two parts, where one continues its trajectory and deposits on the substrate, and the other part remains on top of the mask [50-56].

Laser is an efficient and accurate tool that was introduced to LM patterning recently [57-59]. Since LM has a high absorption of laser energy, the laser beam can selectively and precisely ablate unwanted LM, leaving the remaining LM to form the pattern. Although it can pattern a line down to micron scale [59], the space is limited to a hundred microns due to the transient thermal transmission during the ablation and the high thermal conductivity of LM. In addition, the substrate materials are constrained and should be transparent to laser, and it also wastes LM during the ablation. When the resolution is up to microscale, the substrate needs to be coated with layers of high surface energy materials to fix the LM. In conclusion, direct laser patterning of LM is expensive and difficult to operate because the laser beam easily damages the pattern due to the LM's high-energy absorption and thermal conductivity, and the contaminated substrate would influence the following encapsulation.

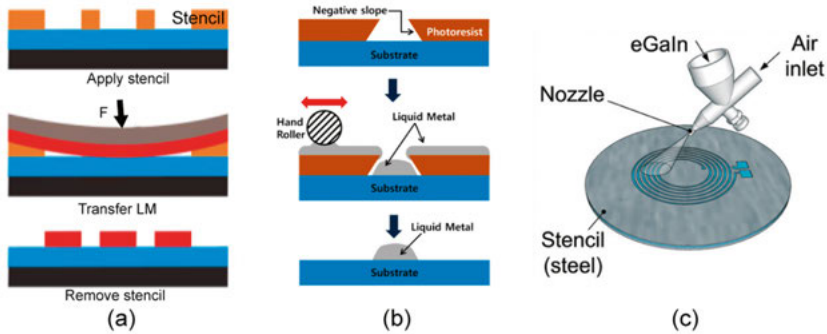


Figure 4. Masked deposition. (a) Cutter plotter produced mask (Reproduced with permission from ref. [50]), (b) photolithography defined mask (Reproduced with permission from ref. [55]), and (c) Steel stencil (Reproduced with permission from ref. [56]).

Among the above-mentioned patterning techniques, masked deposition is one of the most popular since it has an excellent capability to broaden the range of allowable circuit geometry. For example, a shadow mask can incorporate lines with variable widths and angles, isolated patterns, and can adjust the circuit diagram's density and resolution. More importantly, it is a parallel processing

technology, which is better suited to high-volume production. Researchers have developed several types of shadow masks for LM patterning (Figure 4), but the following considerations can expand printing applications in skin-skin electronics further.

- 1) High-resolution and high-density patterns can enable smaller sensors and circuits for modern chips with small pitch and pad size.(for 01005 passive components, the distance between pads is as small as 127 μm , and for the ultra-fine pitch chip scale package, the ball grid pitch is 0.3 mm and the pad size is 0.15 mm).
- 2) High-density and complex pattern diagrams with closed-loop features or arbitrary geometry demands a sacrificial mask.
- 3) Lower costs enable wider applicability.

1.3.2 Patterning with particles

For all techniques above, the separation of LM from the bulk plays a critical role for high-quality patterning. In direct patterning, the nozzle or microchannel extrude the bulk LM into a filament in size down to the tens of microns. And the sticky oxide layer provides a force to drag the filament to separate. In masked spray deposition, the separation happens at the orifice, where the bulk LM is broken and separated into small droplets by the high-speed gas flow. Similarly, the thermal shock triggered by a laser beam could remove and separate the wanted and unwanted LM.

One point in common to them is that they all build the pattern from bulk LM. When doing so, the high surface tension and flowability can cause instability and variation during the separation in the patterning. This instability influences the printing process in various aspects, such as in resolution, complexity, precision and repeatability, and especially when the size of the features is down to a few tens of microns. Therefore, building the conductive pattern from micron/submicron particles can be an attractive way to solve this problem.

Liquid metal micro/nano particles can be produced in a variety of ways, including molding (mm), acoustic waves (10-100 μm), microfluidics (μm), mechanical stirring (micro/nano, large variation), and sonication (micro/nano). The agitation from these methods initially separates the bulk LM into particles. A self-assembled monolayer (SAM), formed on the particle's surface by the reacting with surrounding substances like oxygen or solvent, can stabilize the particles. With continuously agitating, the particle size becomes relatively more even and smaller until certain limitations [60].

Sonication, which contains acoustic cavitation forming and implosive collapsing during the sound waves propagating, is a complex process but an effective way to produce micro/nano LM particles [61]. The collapse continuously breaks the LM into micro/nanoscale sizes, and the synchronous chemical reaction stabilizes the particles by a double-layers shell [62].

The sonication-produced SAM forms a viscoelastic shell around the liquid core. It consists of an organic substance, which cause electrical insulation. Hence, it has to be ruptured to coalesce particles, to create an electrically conducting layer. However, this is difficult due to their particular structures of viscoelastic shell, high surface tension, and micro/nano dimension. The basic coalescing and merging principle is to make the droplet deformed so much that the surface strain exceeds its fracture limit and rupture. Since the surface to volume ratio is the smallest for a sphere, when the core-shell droplet becomes deformed, the shell will become strained and rupture, and then enclosed pure LM merges to form a conductive pattern.

Several strategies have been developed to fuse LM particles [60-70], as shown in Figure 5. The deformation has been achieved by pressure applied from a tip or expansion from a transient temperature change. As shown in Figure 5a, one way was to have the LM particles encapsulated inside the soft polymer channel, and enforce coalescence by applying a compression force. The compression can be provided by a knife [65] or a micro-scale probe. This force can also come from squeezing the channel wall, triggered by stretching of the chips [68] or thermal expansion of substrate [70]. As illustrated in Figure 5b, the particles were evenly paved on a soft substrate and then selectively activated by a robot-controlled soft nozzle tip. The path that the head passed through became conductive, presenting an automatic patterning technique. Laser can bring abrupt energy changes in the order of nanoseconds in local areas. When irradiating to LM particles, the laser can cause local rupture and merge with the effect of thermal expansion and shrinkage.

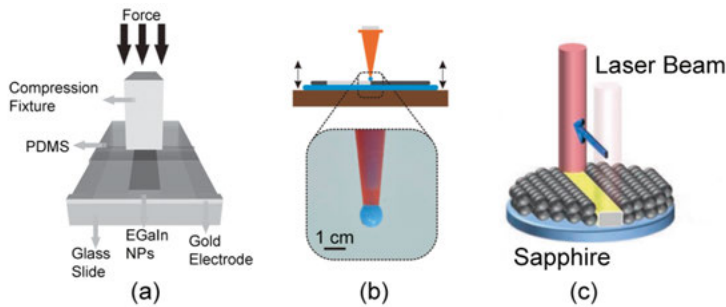


Figure 5. Patterning with micro/nano particles. (a) Sintering with pressure after encapsulation. (Reproduced with permission [62]). (b) A soft nozzle tip for pressure merging (Reproduced with permission [64]). (c) Laser activating merging (Reproduced with permission [67])

These techniques demonstrate that patterning LM conductive lines from micro/nanoparticles is promising. The studies of these techniques focused on the merging principles instead of on the patterning. One issue is that, just like other printing techniques with linear scanning, the serial processing cannot reach the high throughput as batch processing provides. In addition, they only provide high fidelity on planar substrates, limiting the applicability for printing on more complex shapes of a carrier. Hence, the advantages of making LM patterns from particles have not been fully explored and exhibited.

1.4 Scope of the thesis

Soft electronics, and especially conformal skin-like electronics, build a bridge to allow us to sense and communicate with soft tissues like human skin, soft robotics, prosthetics, fragile plants, small and delicate organisms, *etc.* Liquid metals are attractive materials to build a soft and stretchable architecture due to the unlimited stretchability of a liquid and its high conductivity. Moreover, its self-healing property, which means that its conductivity can recover after damaging, distinguish it from other stretchable conductors. However, with the difficulties arising from its high surface tension, fluidity, and instantaneously formed passivated oxide layers, many ways of patterning technique have been studied but there are still needs for better understanding and new solutions to fully harness its potential in soft and stretchable skin-like electronics.

Masked atomization and deposition (Figure 6a) of liquid metal is attractive since it is a batch process that may pattern highly dense and complex circuits on various elastomer substrates. However, it had relative low resolution and high variability because of the manual lift-off process and unevenly atomizing process, which are mainly caused by the choice of shadow mask, and atomizing mechanism, and the robust oxide skin and high surface tension of the liquid alloy.

Paper I focused on the fabrication of high-resolution epidermal electronics by introducing a sacrificial mask to improve the lift-off process. This study proposed a technique that can print complex and high-density LM patterns on thin stretchable substrates. It involves ultraviolet laser patterning a modified water-soluble mask, spray depositing liquid metal, automatically lift-off in water, and component integration and encapsulation. With this new technique, it was possible to make epidermal precision strain sensors with high-density LM patterns capable of monitoring fine local skin movements like the detailed process of wrinkles forming, releasing, and joint motion.

a) Masked deposition

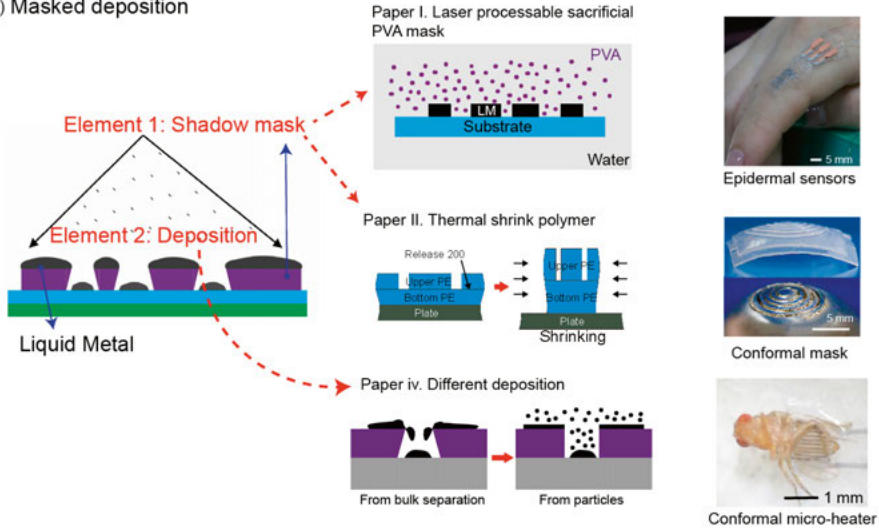


Figure 6. The printing techniques studied and their enabled stretchable skin-like electronics. The main elements of this thesis are (a) masked deposition, and (b) transfer printing.

The mask resolution is often constrained by the processing equipment, and its fabrication cost increases drastically with increased resolution. Paper II proposed a masking technique based on a shrinkable film that can make high-resolution masks using a mechanical cutting plotter together with an ordinary oven. After shrinkage, the mask pattern's width and space can reduce to the dimension that is about one-third of the original cut pattern, with potential to go even smaller. To better predict the final structure, several parameters were investigated experimentally and numerically. Moreover, the final mask could be transferred to non-planar surfaces like cylinders or spheres.

Due to the random and chaotic nature of the atomizer spraying process and the high surface tension of the LM, it is hard to have high precision at high

resolution. An alternative approach is to build up the pattern from micron/sub-micron particles. Unfortunately, without intervention, coalescing sprayed particles is challenging due to their small size and core-shell structures, and the wetting of the particles. Paper III, we proposed a proper way of employing collision-caused rupture and sintering. The merging mechanism was studied with a high-speed camera and a scanning electron microscope (SEM). With this technique, we fabricated a compliant micro-heater with high density and resolution, which could thermally activate ectopic expression of enteroendocrine cells in local abdomen of *drosophila*.

Flexography printing is common in the conventional printing industry. By tuning the wettability of liquid metal to substrates through a selective surface morphological modification, we presented a flexography printing technique to enable patterning of liquid metal circuits on both planar and complex 3-D surfaces, and investigated the tuning mechanism and the relation between the wettability and surface morphological modification.

In order to enable sensing on fragile and delicate plants, in paper IV we proposed a gentle hydroprinting technique to pattern compliant electronic on plants that could sense physiological signals and even function as a biohybrid to determine plant behaviour on demand. Functionally, the conformal architecture could monitor leaf moisture content and length, and be used to manipulate leaf and bean sprout orientation (Paper V).

In summary, my objective was to explore LM patterning techniques for the potential application of LM based soft and stretchable skin-like electronics. This thesis proposes several approaches to patterning LM in microsystems. Materials and printing mechanisms were investigated and characterized. Final devices have been demonstrated in several applications.

2. Materials and processing techniques

2.1 Materials

2.1.1 Liquid metal

Liquid metal is liquid at or near room temperature, which has metal and fluid properties, like high electrical and thermal conductivity, and high fluidity. Due to its non-toxic and zero vapour pressure at room temperature, gallium-based liquid metal or liquid alloy is amenable to many applications [71-72]. Two commonly used gallium based liquid metals are Gallium, Galinstan (approximately, 68.5% Ga, 21.5% In, 10% Sn, with small amounts of Bi or Sb), and GaIn (75% Ga, 25% In). They have a silvery and glossy surface and shape like a viscous liquid (Figure 7).

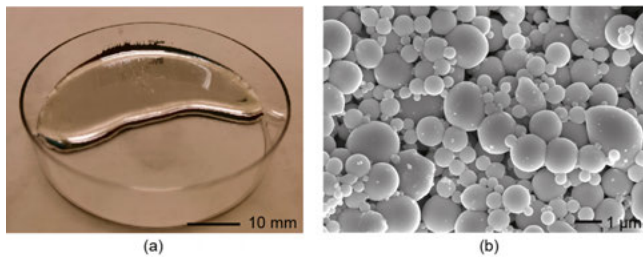


Figure 7. Liquid metal morphology. (a) A liquid metal (Galinstan) puddle at room temperature in air. (b) LM particles produced with sonication.

In this thesis all LM are gallium-based liquid metals (Table 1). Although the conductivities of them ($\sim 3 \times 10^7 \Omega^{-1}\text{m}^{-1}$) are about one-tenth of copper ($3 \times 10^6 \Omega^{-1}\text{m}^{-1}$) or silver ($3 \times 10^6 \Omega^{-1}\text{m}^{-1}$), it is much higher than other fluidic conductors, which contain liquid medium and conductive additive.

Table 1. Properties of liquid metals.

Composition	Galinstan	EGaIn	Hg
Melting point (°C)	-19	15.5	-38.8
Boiling point (°C)	>1300	2000	357
Density (Kg/m ³)	6440	6280	1353
Electrical conductivity (S/m)	3.46×10^6	3.4×10^6	1×10^6
Viscosity (Pa·s)	2.4×10^{-3}	2.0×10^{-3}	1.5×10^{-3}
Surface tension (N/m)	0.718	0.624	0.487

LM is an incompressible fluid with low viscosity (bulk modulus 24.6 GPa and viscosity $\sim 2 \times 10^{-3}$ Pa·s, *cf.* water has 2.1 GPa and 0.9×10^{-3} Pa·s at room temperature), which makes its response to pressure almost instantaneously. Therefore, it is an ideal conductor for soft electronics.

Gallium reacts with many metals and strongly with aluminium. In addition, gallium instantly reacts with oxygen even at low concentration [71]. This typical oxide layer mainly consists of Ga_2O_3 , which is a passivated oxide, and has a thickness of ~ 3 nm [73-74]. The strong adhesion of the oxide makes LM contaminating almost any surface. Its high adhesion enables printing LM on soft materials, and even when the material does not wet oxide-free [36]. As shown in Figure 8, the receding angle of LM on pure PDMS surface is quite low, although its static angle is LM-phobic.




Contact angle Substrate	Static angle	Advancing angle	Receding angle	$\theta_{\text{adv}} - \theta_{\text{rec}}$
PDMS	144.3°±0.7° 	153.7°±1.3° 	9.5°±0.8° 	$\sim 144.2^\circ$

Figure 8. Photographs of contact angle.

A variety of fabricating methods can produce LM particles with variable sizes, ranging from nm to mm. Micro/nano particles of LM (Figure 7b) have been developed to deliver drugs or lump curing [75-76].

2.1.2 Polyvinyl alcohol

Polyvinyl alcohol (PVA) is non-toxic, tasteless and harmless to the human body. More importantly, it is a water-soluble polymer and is friendly to the natural environment. Due to its biocompatibility, low tendency for protein adhesion, low toxicity, it has wide medical applications, including cartilage replacements, contact lenses, and eye drops [77-79].

PVA film is characterized by good compactness, high crystallinity, good flexibility, oil and organic solvent resistance, abrasion resistance, and good gas barrier properties. It is widely used in the market since it is a green and environmentally friendly functional material that can be completely degraded by microorganisms in the soil. It can be degraded into carbon dioxide and water quickly and has the effect of improving the land.

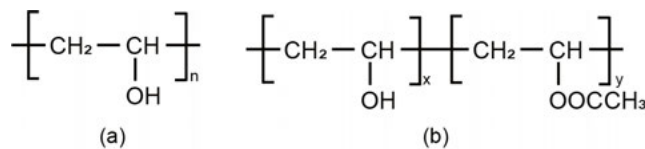


Figure 9. Polyvinyl alcohol formula. (a) Completely alcoholysis PVA. (b) Partial alcoholysis PVA.

The biggest advantage of PVA is that it is water soluble because of the hydrophilic hydroxyl group in the molecule. The solubility is influenced by the degree of polymerization (DP) and alcoholysis at the molecular level. The DP is the number of monomeric units (Figure 9a) in a macromolecule. The lower DP contributes to easier dissolvability. PVA with 500 DP can dissolve in water at room temperature, while it would take 2~3 hours at 80 °C for 1700 DP. Part alcoholysis of PVA (Figure 9b) has higher solubility in water than full alcoholysis. The degree of alcoholysis indicates the mole percent of hydroxyls. For example, 88 moles % PVA has good dissolvability, but 99% does not.

There are other considerations for making a PVA shadow mask, such as film-forming ability, film stripping, and flexibility. High DP leads to considerable cohesion, making the film stiff and even bending due to stress concentration. Part alcoholysis has much higher flexibility. Therefore, we selected 0588 (DP 500, 88 mole %) in this thesis.

Moreover, water is non-toxic and environmentally friendly, and can dissolve PVA without causing any negative effects on the silicone elastomer substrate. In contrast, organic solvents (such as ethanol and isopropyl alcohol) can trigger severe swelling deformation of silicone elastomer.

The PVA film thickness is easily adjustable via the fabricating process, ranging from several to hundreds of microns. Mask thickness is an important factor in determining the cross-section geometry and depositing resolution. Thus PVA film is an excellent option to fulfill this requirement. For example, when the cutting tool is fixed, the thin film can provide a lower aspect ratio, creating a better pass-through condition for LM deposition. For skin-like electronics, the thin PVA film could enable the patterning in microscale.

2.1.3 Silicones

Soft electronics have high mechanical compliance to the soft and stretchable surface, such as human skin, soft robotics, soft tissue, fragile plants, or small and delicate organisms. Polydimethylsiloxane (PDMS) like Sylgard 184 (Dow Corning) and Ecoflex 30 (Smooth-On), which are commercially available, has physical properties (Table 2) close to these soft systems. As the substrate, they are transparent, inert, and mechanically robust. In addition, the polymers have suitable electrical performance, such as low dielectric constants and relatively low hysteresis between loading and unloading cycles. To sum up, these elastomers quite well meet the demands for soft electronics.

They are made by curing two liquid components, a silicone oligomer (base) and cross-linker. The PDMS can be cured into replicas by molding and into a thin film with an applicator. The properties of PDMS (Sylgard 184) can be tuned by varying the stirring time, curing temperature or time, and additives [80].

Table 2. Mechanical properties of three elastomers.

	Sylgard 184	EcoFlex00-30	S3-PDMS	Human skin
Stretchability	100%	900%	150% [80]	30%~60%
Young's modulus	1 MPa	35-69 kPa	24 kPa	10~47 MPa

* The skin properties depend on the body part, the age of the person, and the stretching speed in testing [81].

2.1.4 Shrink film

With the relaxing of the polymer chain, shrink polymer film can shrink to a specific ratio after heating. During manufacturing, the original entangled polymer chains have been orientated stretched. With heating, the polymer chains reorganized to their original random pattern [82-85]. The degree of shrinking is approximately equal to the stretch ratio of the orientation process.

Polyethylene shrink film is a thermoplastic polymer with a variable crystalline structure. Shrink films are commonly used for packaging applications. After shrinking, the original loose cylindrical package would be conformally covered on the object surface as a protective or encapsulating layer. With features such as being soft, easy to process, and available in various thicknesses, it is well-suited as a stencil mask for depositing atomized liquid alloy, various inks, prepolymers, or paints.

With different pre-stretched methods and parameters in manufacturing, the shrink polymer film could shrink uniaxially or biaxially with different shrink ratios. In addition, the shrink ratio could be precisely controlled by adjusting the processing parameters in shrinking, including temperature and time, which allow the mask to obtain a variety of results.

2.2 Mask fabrication

2.2.1 Sacrificial PVA mask

Due to the low absorption in pure PVA with the ultraviolet nanosecond laser, dyes were incorporated in the polymer to enhance the absorption and lower the cutting threshold. We introduced two kinds of pigments, one is water-based blue ink, and the other is acetylene carbon black. These pigments were directly mixed with the pure PVA solution and poured on acrylic or polyethylene terephthalate (PET) substrate for curing, as exhibited in Figure 10.

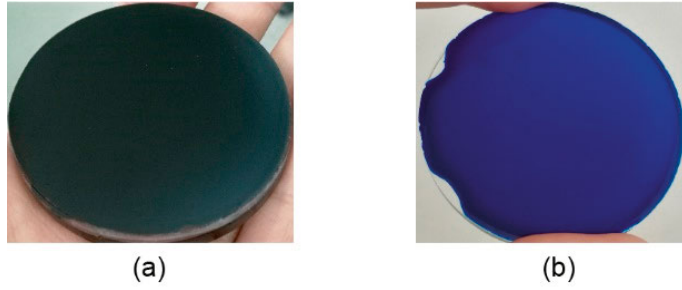


Figure 10. A PVA film with different pigments (The substrate is 60 mm in diameter). (a) Carbon black. (b) Blue ink.

Laser cutting is a mature technology for patterning PCBs because it is highly efficient when small series and not very long patterns are required, it is easy to use, and environmental friendly. A UV laser (LSU5EI; HGtech) with a minimum beam spot about $25\ \mu\text{m}$ was selected to engrave the mask.

Figure 11a exhibits a mask that was cut with a scanning speed of $70\ \text{mm/s}$ at a repeating frequency of $80\ \text{kHz}$. The intensity distribution of the laser beam is not evenly but Gaussian distribution. Therefore, the sidewall of the channel is not vertical but a reversed quasi-trapezoid. In addition, the laser power should be adapted carefully, since excessive energy (Figure 11b-c) would affect the patterning quality in the subsequent processes.

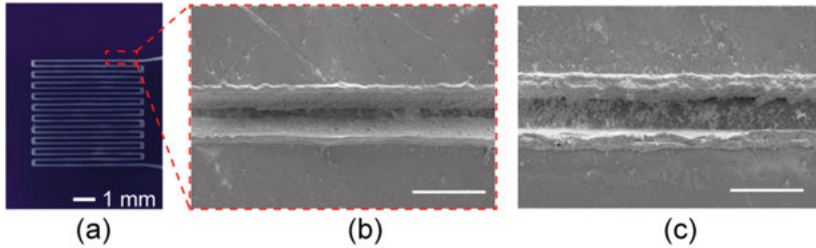


Figure 11. Laser cut mask. (a) PVA mask, the white line is the open channel. SEM images of laser produced line. Less melting residue (b) and over-melting residue (c). The scale bar is $100\ \mu\text{m}$.

2.2.2 Shrink film mask

A simple masking technique (Figure 12a) was developed, which could improve the resolution and change the shape of the originally cut shadow mask for liquid metal deposition. First, a mechanical cutting plotter cut a pattern in the original shrink film on a PDMS substrate. PDMS could provide good adhesion to fix the shrink film for precise cutting. Then this mask was aligned with an un-patterned underlying shrink film so that the film below could effectively drag the top surface pattern to shrink conformally. After shrinking in the oven, the shrunk mask was transferred to the target substrate for LM deposition and encapsulation.

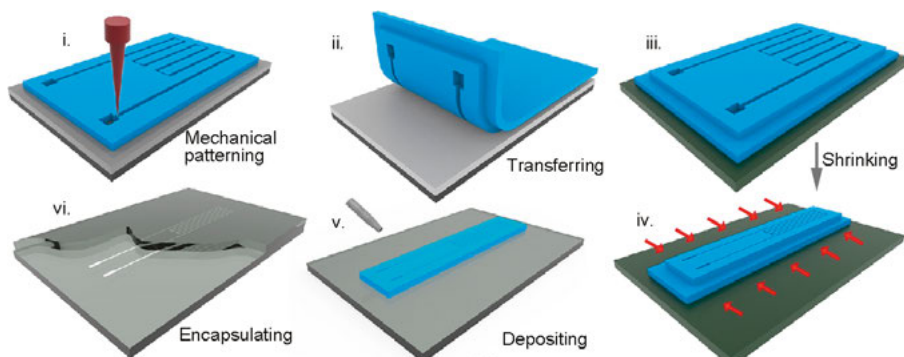


Figure 12. Shrink mask fabrication and LM patterning process. (i) Pattern the original shrink film. (ii) Two layers shrinkable films align and transfer. (iii) Place the double-layer structure. (iv) Shrink in the oven. (v) Deposit liquid metal (vi) Encapsulate the pattern.

The polymer chain is pre-stretched during its manufacturing, so the mask resolution will be enhanced several times after releasing in high temperature. The cutter plotter could reach resolution with $100\ \mu\text{m}$ in width and $200\ \mu\text{m}$ in space. After shrinking, we could find that the width and space could down to 35 and $60\ \mu\text{m}$, respectively, which is about $1/3$ of its original dimension. As shown in Figure 13a-b, the open channel width and space in-between could be as fine as 35 and $60\ \mu\text{m}$, respectively. Due to the low adhesion between the shrink film and the PDMS support below, the cutting plotter produced channel width and space can reach approximately 100 and $200\ \mu\text{m}$, respectively. In addition, the resolution was also limited by the increased aspect ratio of the cross-section when shrinking (Figure 13d). When the aspect ratio was too high, the structure became unstable and falls down.

Figure 13c-e exhibit both uniaxial and bidirectional shrinking behaviour. The original squares and circles are transformed to rectangles and ellipses with 70% uniaxial shrinkage. If the pre-stretching is in two orthogonal directions, the shrinking will be nearly homogenous. Figure 13f exhibits two different final masks that are actually from the same original pattern. On the other hand, this result also indicates that isolated patterns could be shrunk without destroying the entire structure.

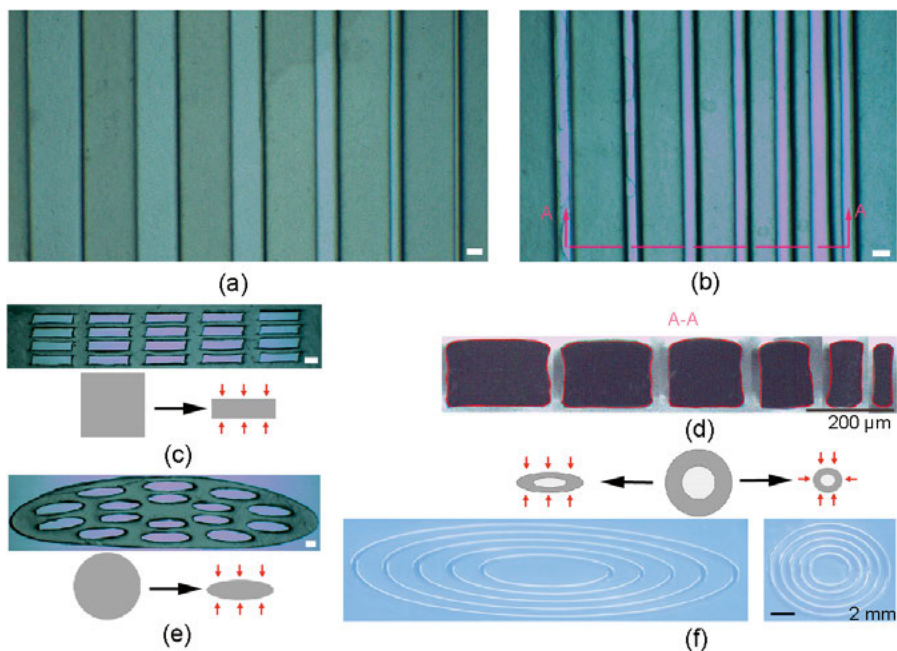


Figure 13. Shrink masks. The scale bars mark 100 μm , and the red arrows indicate the contract direction. (a) The widths of channel are 34, 68, 136, 221, 284, and 358 μm , shrunk from the original 100, 200, 400, 600, 800, and 1000 μm , respectively. (b) The spaces are 60, 113, 173, 240, 298, and 349 μm , shrunk from the original 200, 400, 600, 800, 1000, and 1200 μm , respectively. Examples of the formation of matrix with rectangles (c) and ellipses (e) are shown in the diagram below. (d) The cross-section of A-A in (b). (f) Shrink masks from the same pattern but of different shrinkage anisotropy.

The bottom PE layer plays a critical role in finishing these isolated patterns, which could be considered a buffer to reduce the friction between the top film and the bottom plate. It helps to maintain the dimension and relative gap during the whole shrinking moving process. That is because the thermal-induced shrinking force is relatively weak compared to the friction from the bottom. We conducted a comparative experiment to illustrate the importance. Figure 14 shows a representative pattern, which has a rectangle shape with a triangular opening and a narrow stripe on its right. Its right stripe since all the area would shrink towards the centre. Shrinking from the same original pattern, we find the left mask with the bottom support can have an expected and undistorted shape from both simulated and experimental results.

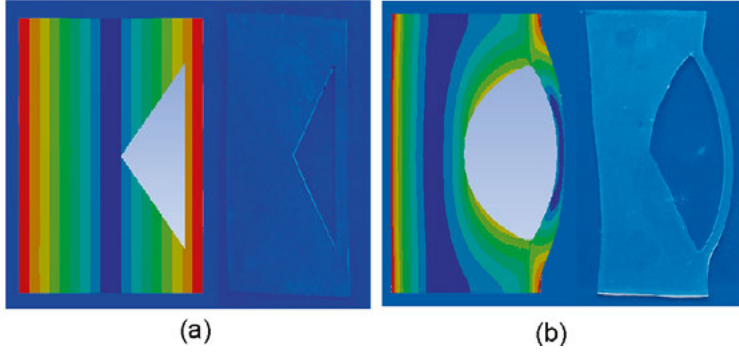


Figure 14. Bottom layer function explanation. The shrunk masks with (a) and without (b) a bottom aligned shrink film. The colour illustrations are FEM simulation results, and the transparent shrink films are experimental results from the same original pattern.

To understand the shrinking, we studied the relationship between the time and shrinkage at a set temperature (140 °C) in the oven (Figure 15a). A slight expansion occurred at the beginning due to thermal expansion. After that, the shrinking accelerates exponentially with time. After that, the curve becomes nearly flat, since almost all stored pre-stretch is released. Due to the thermal inertia, contracting slightly continues after taking the film out from the oven. A group of shrunk mask were measured as shown in Figure 15b. It shows the relation of shrinkage versus time and temperature. With increasing temperature, the final shrink ratio became higher until it stabilized at 145 °C. Although the total shrinking time varies under different conditions, the main contraction processes is completed in about 1 min.

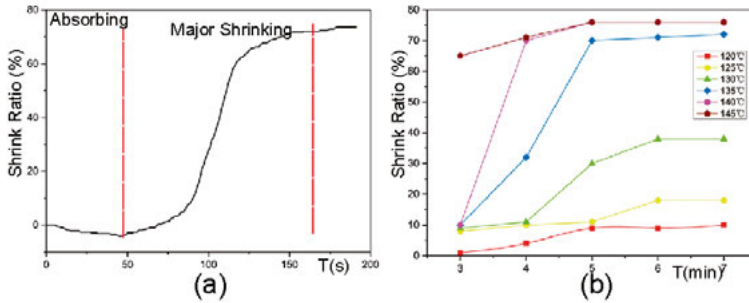


Figure 15. Shrinking process investigation. Shrink ratio versus time (a) and temperature (b).

Figure 16a exhibits a packaged strain sensor patterned by a shrunken mask, which has a channel with 100 μm in width contracted from the original 200 μm . An elliptical spiral pressure sensor (Figure 16b) was also deposited, using a uniaxial shrinkable film contracted from a right circular spiral pattern. Furthermore, we find that this technique can be applied to fabricate non-planar mask. When the shrink becomes the gel-like state, it could conformally lay on

the bottom 3-D surface, either cylindrical or sphere surface, as displayed in Figure 16 c-d. The process for the sphere is slightly modified, which require another new PE film to wrap the entire structure to push the mask shrinking toward the steel hemisphere surface. We could optimize this process by introducing a platform that could uniformly apply pneumatic or hydraulic pressure to the PE film surface. It is possible to fabricate conformal masks for more complex 3-D characters.

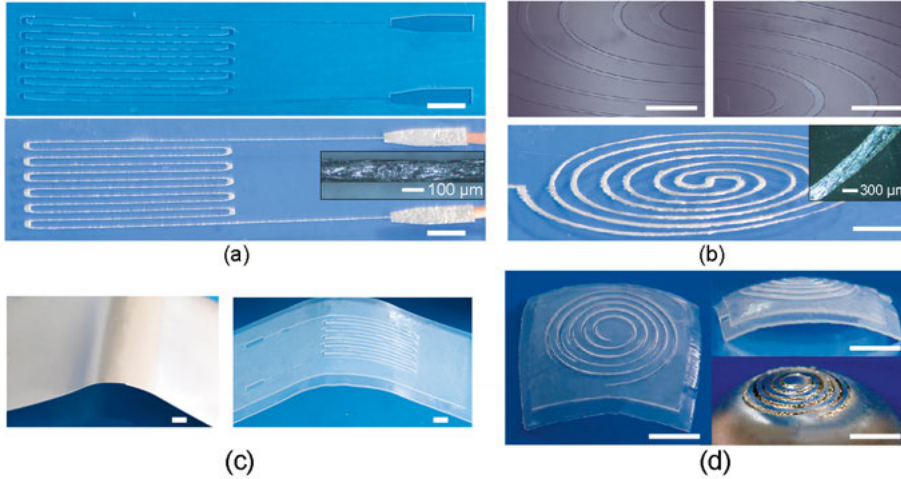


Figure 16. Shrunken PE masks and deposited patterns. The scale bars mark 5 mm. (a, b) The uniaxial shrunken PE mask and deposited sensor, the inset is the local circuit micrograph. (c) Cylindrically curved mask. (d) A hemispherical spiral mask.

2.3 Lift-off patterning

2.3.1 The processing technique

The process is schematically depicted in Figure 17. The PVA film is patterned by laser and transferred onto a semi-cured PDMS substrate. With atomized spraying, the LM is deposited and exposed after water dissolving lift-off process.

We have introduced a one-time transfer technology. The transfer tape, a thin semi-cured PDMS on a PET film, works either as a substrate or as an adhesive to bring the pattern from the silicon wafer. We found that semi-cured PDMS has a larger adhesion than that between the mask and its supporter. Therefore, the mask can be peeled off and then transferred to the target substrate with one-time transfer. This strategy greatly simplifies the transfer processing and assures high-quality masking.

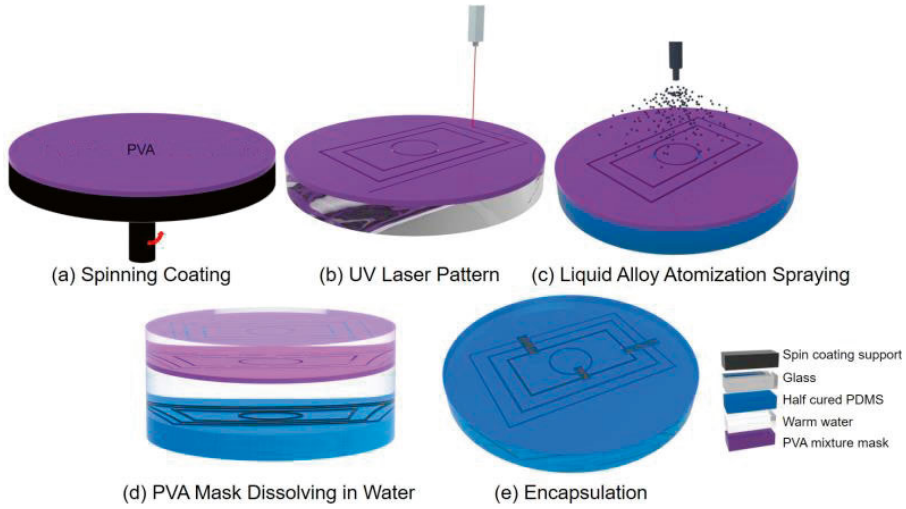


Figure 17. Schematic illustration of the critical processing steps. (a) PVA film manufacturing, (b) laser cut the PVA mask, (c) transfer the mask and deposit liquid metal on the mask, (d) dissolve and rinse the mask in water, and (e) dry and encapsulate.

More importantly, with this operation, the mask cross-section is flipped upside down so that the opening gets an inverted profile, which exactly meets our demands for the subsequent lift-off process. Figure 18 schematically illustrates the lift-off process, which is the critical part of this process. Due to the Gaussian distribution of the laser spot, the cross-section of top is wider than bottom when cut by the laser, making the top opening smaller with sharp edges after one-time transfer.

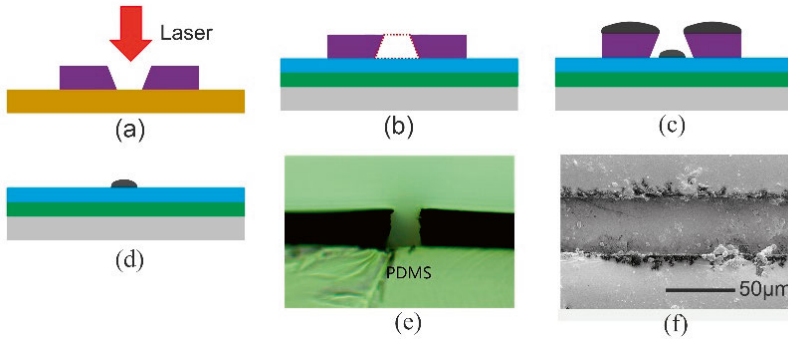


Figure 18. Lift-off process illustration. (a) Laser cut cross-section. (b) Inverting trapezoid. (c) Liquid metal separation. (d) LM exposing. (e) The inverting trapezoid micrograph. (f) Separation line on SEM image.

Due to the high surface tension of LM, its inner cohesive force is strong enough to make the atomized LM droplets reconnected after depositing to the substrate. The sharp edge plays a critical role to separate the deposited LM on

the mask and from that on the substrate. Assuming the transition from the top to the bottom is inclined so that the LM will cover it, the LM would form a continuous film, leading to a damaged pattern during the lift-off process. The SEM image from the top view (Figure 18f) reveals the separation line between the masked and unmasked regions. In addition, the amount of deposited LM should be controlled. Although inverted profile with a sharp edge can separate thin film, once the LM thickness exceeds the mask height, the deposited LM will form a continuous film.

2.3.2 Performance characterization

With the sacrificial mask, various LM patterns are exhibited in Figure 19. The smallest LM line width and space are 30 μm and 40 μm , respectively. The limitation is determined by the laser spot and the mechanical properties of the PVA. PVA residues generated during the laser cutting could reduce the pattern quality during the PVA mask transferring, as it will not form a tight contact where the residue hinders the contact. Figure 19 c-d exhibit the possibility of fabricating isolated pattern, which is necessary for complex circuits. Although the smallest dimensions showed promise, we could see much LM residue attached to the patterned line, which was caused by the uneven atomization of spraying bulk LM.

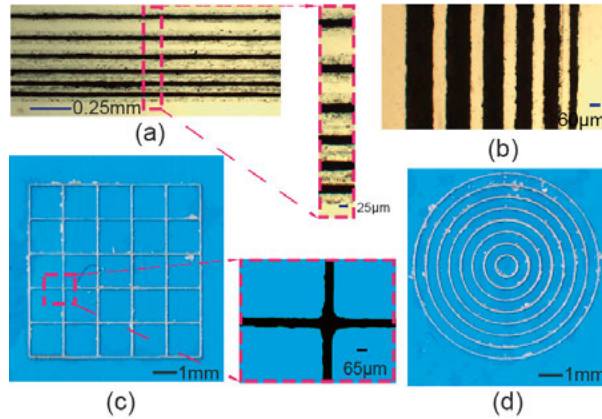


Figure 19. Various LM patterns. (a) A group of 30 μm width lines with different space from 40, 50, 70, 90, to 110 μm , and a zoomed micrograph, (b) the line width varies from 40, 60, 80, 100, 120, to 140 μm with the same space of 60 μm , (c) The grid with 65 μm width of LM line, and (d) A group of concentric circles varied from 1 to 8 mm, LM width is 65 μm .

From the fracture test in Figure 20, we can find that the fracture occurred just after 100% strain, which is exactly the tensile strain of Sylgard 184. This indicates that our technique has no negative impact on the material itself. A matrix of LEDs connected by LM shows stable performance under stretching,

twisting and bending, demonstrating the ease of such hybrid integration, Figure 21.

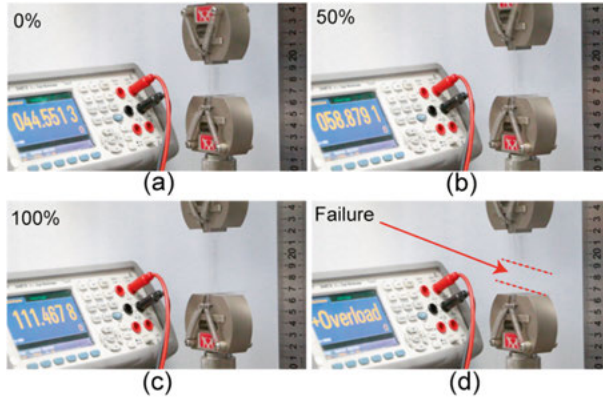


Figure 20. Fracture test. A patch is stretching from zero strain to its fracture.

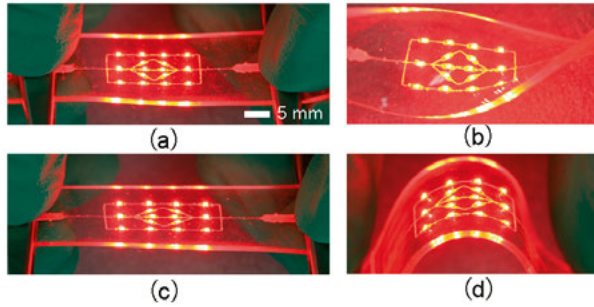


Figure 21. An array of LEDs with a soft and stretchable interconnector. (a) in its original shape, (b) twisted, (c) stretched, and (d) bent.

The contact between liquid metal and rigid components needs to be investigated due to the existence of LM oxide layer and the protective coating layer on the component. These layers would inhibit or weak the electrical contact in-between. Once the contact is not stable, it will severely influence the electrical performance and cause either a high contact resistance or an unstable connection, especially under stretching. Because of the less contact area, these problems could become more severe when the contact is in high resolution.

A pair of copper electrodes integrated with an LM-based strain sensor was fabricated to test the repeatability and stability of the contact. The tensile fracture strain and the cyclic strain were driven by a dynamic tensile system (E1000, Instron, USA). Figure 22b indicates that when the copper electrodes are not involved in stretching, the resistance variation is stable during cycling strain from 0 to 50% over 10,000 times. It is interesting to find that the device became a little longer (1-2%) after 10,000 cycles but recovered to its original size after a few days. However, when the copper electrodes are involved in

stretching, it keeps changing gradually and becomes failure at around 880 cycles. From the results, we can find that the resistance change is stable during the first 200 cycles. The resistance starts to change vastly at about 200 cycles because the copper has detached from the bottom thin PDMS layer ($40\text{ }\mu\text{m}$) during the high strain, leading to the leakage of liquid alloy. When the amount of liquid metal is insufficient to connect the copper and circuit, the resistance becomes infinite after 880 cycles. With thicker PDMS reducing the local strain, the contact is supposed to survive longer. The contact damage is essentially caused by the considerable difference of Young Modulus between stretchable elastomer and the rigid metal components.

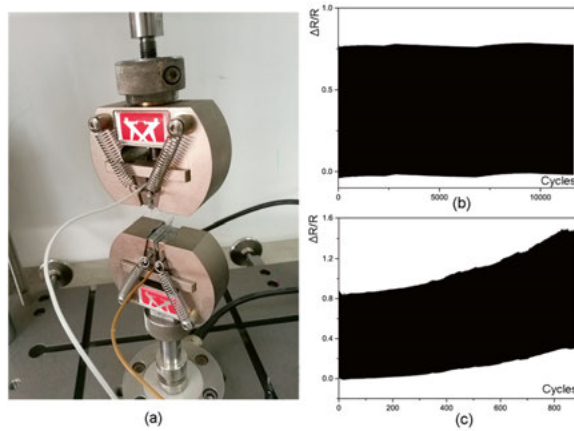


Figure 22. Contact stability test under 50% strain. (a) A dynamic tensile system. (b) Stretch cycling test when the copper is not involved (b) or involved (c).

2.4 Deposition with liquid metal particles

2.4.1 Liquid metal particles

The ink was prepared by sonication of Galinstan in ethanol solvent. With a change in sonicating time, the size distribution also changes, and the details are listed in Figure 23. In general, the average diameter becomes smaller and size distribution becomes narrower as the time prolongs. In addition, the particles number below 800 nm takes a large ratio. However, the large particles occupy more volume, which contributes more to the LM circuit composition.

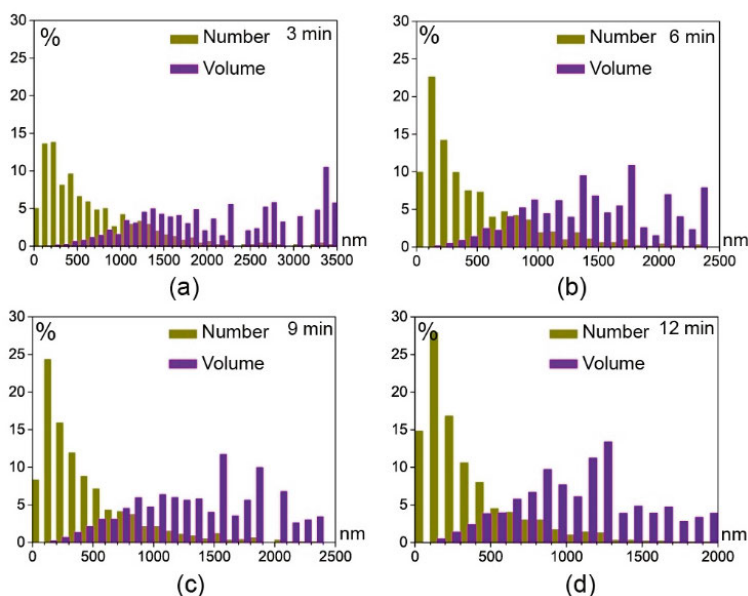


Figure 23. Different size distribution of particles. The particles were produced with varied length of sonicating times, 3 (a), 6 (b), 9 (c) and 12 (d) minutes, respectively.

A reaction between the LM surface and the solvent produced a self-assembled monolayer (SAM). The sonicating produced particle shell structure in particular has two layers. From the images in Figure 24, we can see the two-layer shell structure. Elemental mapping means that the SAM is composed of an oxide layer and organic substances, which is consistent with other's work [62, 85]. We found that this shell can stabilize the ink for a long period. Although the particles can sink after several hours of suspension in ethanol, it is still well dispersed and useful after blowing and agitating the sediment from the bottom of solvent by squeezing a pipette.

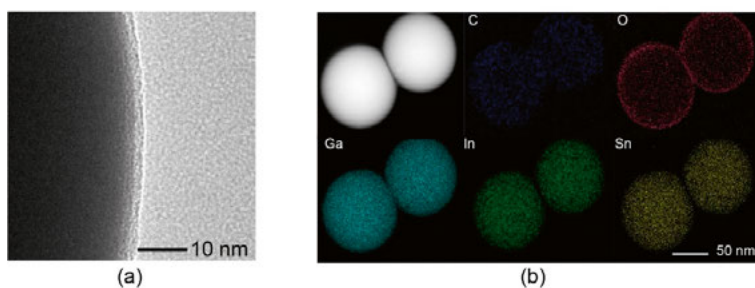


Figure 24. SEM and TEM imaging of LM particle. (a) The two-layered structure of the particle shell, and (b) elemental mapping of the particle.

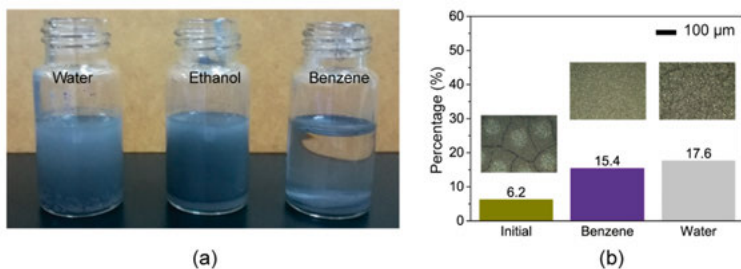


Figure 25. Shell properties exploration. (a) Photographs taken 3.5 h after adding drops of the listed liquids. (c) Micrographs from the bottom view.

Another interesting phenomenon is that, we found that the ink could react with water and dissolved in benzene. After adding water into the ink, there is an clear reaction, generating plenty of small bubbles and leaving chunks of debris. After adding benzene, the initial suspension become clear. Hence, the side-product of sonication could rapidly react with water or dissolve in benzene, Figure 25. It is quite similar to the properties of gallium ethoxide ($\text{Ga}(\text{OEt})_3$) [86]. We believe that Ga or Ga_2O_3 may react with EtOH under the sonication, which produces local high temperature and pressure conditions. In addition, a drop of each suspension was extracted and dried on the glass slide, respectively, Figure 25b. From the results, modified suspensions have a larger shining area. This means that part of the particles had coalesced after the reaction or dissolution, and more inner pure LM was exposed and merged. It is probably that this organic layer probably helps in separating the micro/nano LM particles and maintaining the ink fluidity.

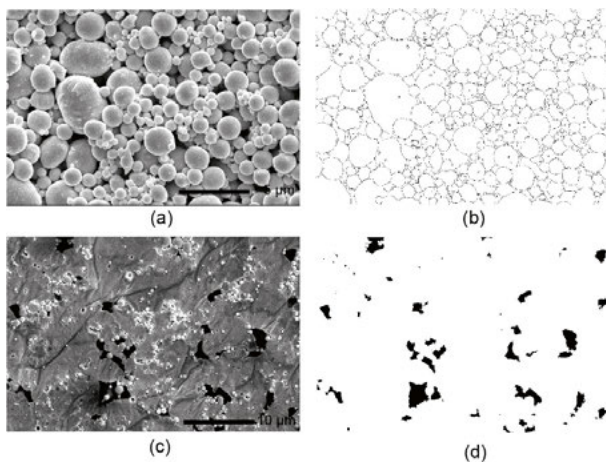


Figure 26. LM particles statistics. (a, c) The SEM images. (b, d) The processed images.

In this work, the statistics like the size distribution of particles and the cover area were acquired by image analysis. The SEM images were firstly processed to segment each LM particle or hole with software MATLAB, cf. Figure 26.

Afterward, the number of particles and the area of the holes were counted and calculated.

2.4.2 LM micron/submicron particles merging

We proposed a technique to coalesce and merge micron/submicron particles by spraying the ink. Here, the evaporation and collision process are the main processes to make the particles ruptured and merged, Figure 27. It is known that a sphere has the smallest surface-to-volume ratio. For LM core-shell micron/submicron particles, once deformed, the viscoelastic shell will become strained. When the strain reaches a critical value, it can induce rupture, and the enclosed LM will be released for merging.

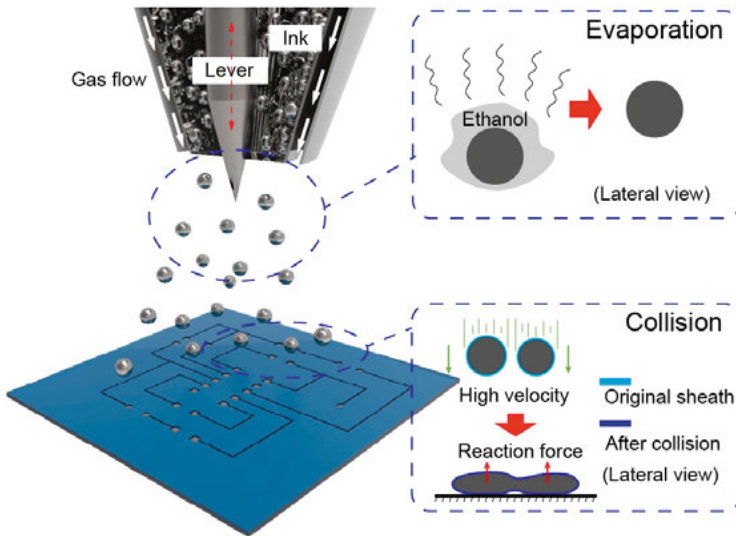


Figure 27. Merging mechanism illustration.

Figure 28a exhibits the produced LM particles suspension ink, and the particles are physically separated. The photo shows the top and bottom of the printed LM film. The bottom has a mirror effect, and the particles have merged to a continuous film. The top displays a spatial morphology, and the low measured resistance indicates good conductivity and demonstrates the particles' coalescing and merging. With normal spraying, the sprayed particles are remaining electrically insulating, Figure 28d.

Coalescence does not always occur; the spraying parameters should be managed scientifically. By varying the printing distance, we found that the deposited film is electrically insulated at short distance, with a sufficient layer of solvent remaining around the particles. However, when the distance exceeds 3 cm (Figure 29a), coalescence occurs and maintains relatively stable between 3-7 cm. At a longer distance, the resistance increases since the film got thinner

as the cone shape of the spray made it spray the same amount of LM over a larger area. The results indicate that the evaporating process is a critical process to induce the coalescence.

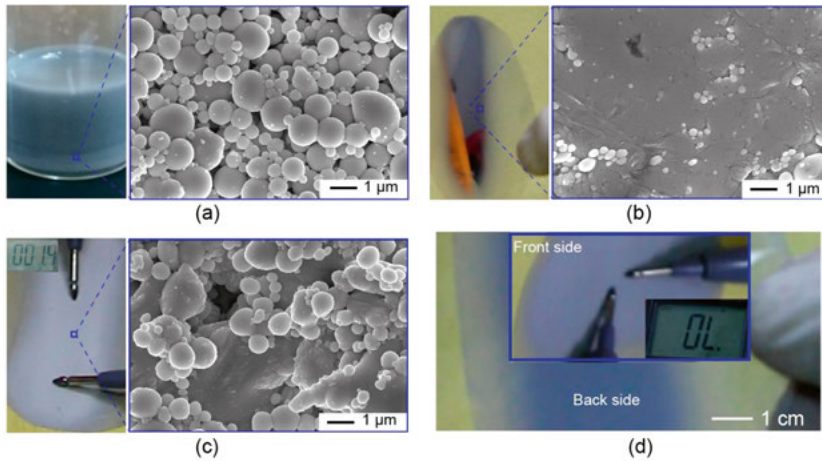


Figure 28. LM particles at different stages of deposition. (a) The produced ink. The top (b) and bottom (c) views of the conductive film. (d) Measuring a non-conductive deposition.

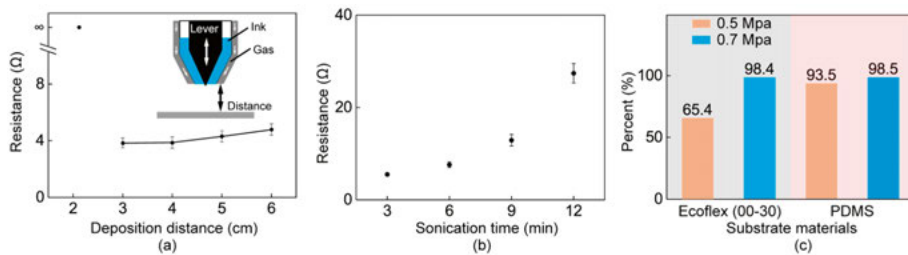


Figure 29. Deposition characterization. The impact of printing distance (a), droplet size (b), and the substrate materials (c).

The particle deformation caused in the collision process can be characterized by four phases: impact, spreading, recoiling, and equilibrium [87-90]. The final equilibrium phase is determined by the area of spread lamella and the adhesion of the sheath. More specifically, the maximum area of the lamella is influenced by the kinetic energy, the size of particles and the Young's modulus of the substrate.

The particle's size decreases as sonication time becomes longer. When the time was less than 3 minutes, the sonication is incomplete and the bulk LM remains. As the particles becoming smaller (Figure 29b), the final resistance becomes larger, since particles needs more energy to get deformed when the size going smaller. The SEM images (Figure 30) also explain the phenomenon, the top and bottom views shows that the number of voids increases with the size decreasing.

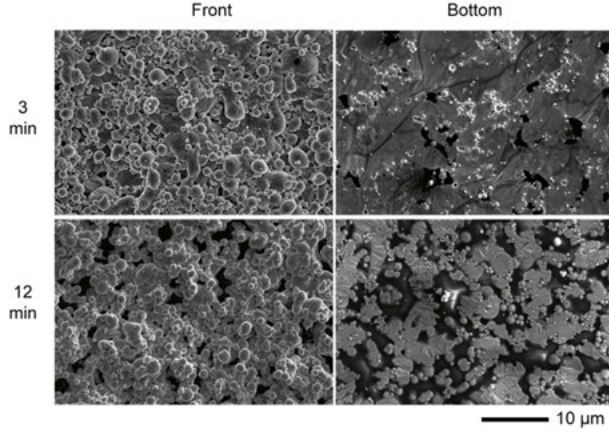


Figure 30. SEM images of the top and bottom views of the deposited LM film.

The kinetic energy for evaporation and collision is provided by the high-speed carrier gas. The necessary energy for each phase can be separately estimated: The reaction force that the particle undergoes during the collision can be estimated according to the momentum conservation,

$$F = \pi \rho \Delta v D^3 / 6t,$$

where ρ is the LM density, Δv is the particle velocity change during the collision, D is the particle diameter, and t is the colliding time.

For a particle with 2 μm in diameter, the minimum reaction force is calculated as 2200 nN. In comparison, following Kramer *et al.* [46], the rupture force for 2 μm driven particles can be deduced to 1600 nN. This comparison indicates that the reaction force is larger than what is needed for rupture. Therefore, the gas velocity could be adjusted to a lower value if the evaporation is accelerated by other means, such as by higher gas temperature, lower ambient pressure, or a solvent with higher vapour pressure.

However, a soft substrate absorbs the kinetic energy and hence reduces the deformation of the particle when it collides with it. We investigated the dependence of the substrate materials by measuring the covered area with the same parameters. When the particles hit different Young's Modulus of substrate, the deposited blob covered area on the stiffer PDMS (Young's modulus: EcoFlex 00-30, $\sim 35\text{-}69\text{ kPa}$; PDMS, $\sim 1\text{ MPa}$) is obviously larger than EcoFlex at 0.5 MPa pressure. With the same material, the cover area increase with the higher pressure and the covered area becomes larger at higher Young's modulus. Since the surface energy of EcoFlex 00-30 and PDMS are very close, this confirmed that the difference of materials truly causes the larger deformation.

In addition to the investigation above, a series of successive micrographs (Figure 31) were extracted from the videos, shot from the substrate bottom side

with a high-speed camera coupled microscope. Initially, several LM blobs emerged separately on the substrate. When increasing in number, parts of them started to coalesce. Finally, all particles merged into a whole structure with a few voids. The blobs imply its capability to establish a uniform deposition in the microscale. At first, the particles spread out on the substrate, and the surrounding substrate was a little concave. If not dry enough, the particle would recoil to a degree under the buffering solvent's impact because of its high surface tension and relatively weak adhesion with the substrate. Then, the stable equilibrium phase was as shown. In conclusion, the LM particles can only be printed on the substrate after sufficient drying.

To explore the shell of the particle, the element variation of carbon and oxygen were investigated with SEM-EDX (Figure 31b). It had been reported that the shell consists of two-layer structures [62, 85], the outer organic and an inner oxide layer. After spraying, we found that the oxygen in the shell increased by 55%, and carbon decreased by 17%. This shown that part of the carbon was gone during the spraying and collision, helping the inner oxide layer stick to the substrate [71-73].

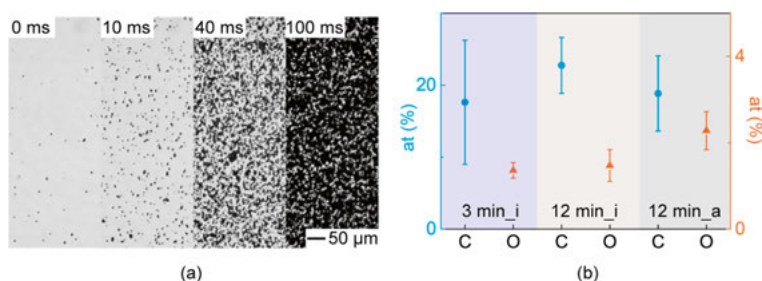


Figure 31. Massive particles merging. (a) Continuous micrographs. (b) The letter “i” is the initial state, and “a” is after spraying.

The monitoring system was the combination of a reverse microscope (DMi 8, LEICA, Germany), coupling with a high-speed camera (V1212, Vision Research, USA), and a light engine (SOLA SM 5-LCR-VA, Lumencor, USA). A 200 μm layer of PDMS was cured on a PET film and then fixed on the top of the objective lens as a substrate for depositing ink. The camera recorded the colliding process from the bottom of the substrate when the ink was sprayed onto its surface directly.

In brief, the high-speed gas flow dry the ink's solvent, and provides sufficient kinetic energy for the core-shell micron/submicron LM particles to hit the substrate and form a continuous LM structure.

2.4.3 Comparison of LM deposition methods

An airbrush (Figure 32) is a typical painting tool used in our laboratory, which basically is a plain jet airblast nozzle. It consists of a chamber containing liquid, externally mixed with air, and a coaxial fluidic channel, one for gas flow and the other for liquid media.

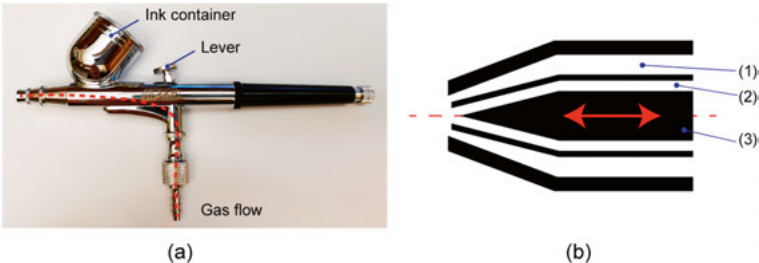


Figure 32. (a) An airbrush bought from market. (b) The coaxial structure of the nozzle. (1) gas channel, (2) liquid fluidic channel, (3) lever needle.

The gas flow meets the ink at the tip, where it breaks the liquid into droplets mainly through capillary action, also known as Rayleigh mode. At a high gas flow rate, the jet from the liquid channel stretches and forms ligaments, which later break into fine droplets due to Rayleigh instability.

Table 3. Major technical difference between the deposition from bulk LM and an ink with particles

	Bulk LM	LM particles
LM size range	Typically several microns with some rare particles of a few hundred microns	Typically one micron with very rare large particles less than 5 microns
LM particles shell properties	<ul style="list-style-type: none">Gallium oxide	<ul style="list-style-type: none">Inner gallium oxide layer and outer organic layerElectrical insulation
Spraying function	<ul style="list-style-type: none">Atomizing bulk LMParticles collision	<ul style="list-style-type: none">Atomizing and evaporating solventParticles collision
Finished LM sheet	Clear pinholes in micro view	<ul style="list-style-type: none">No obvious pinholes.Liquid-solid combined spatial structureGas permeable

Although both techniques are a spraying process, the mechanisms are different, Figure 33. Form bulk LM, the spraying produced particles were actually in an extensive range of distribution, and a small part of them were of several hundred microns in size. Since LM has high surface tension, many areas have more elevated bumps of deposits in macro view and many pinholes in micro

view. In comparison, with its narrow and small size distribution, the LM film deposited from the ink exhibited an even distribution of LM without showing apparent holes.

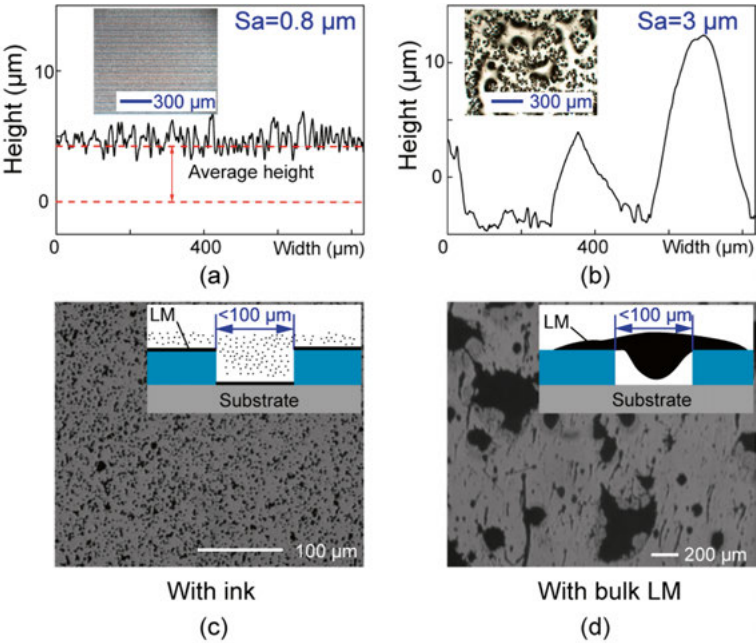


Figure 33. Comparison of two depositions. (a, b) Surface roughness and morphology comparison. (c, d) The pass-through abilities comparison.

A group of LM sheets was deposited on commercial gas permeable substrates (Figure 34) to test the gas permeability. We found that the permeability of sheets produced with ink was much closer to the original substrate than that with bulk LM, even though the light penetration of a sheet sprayed two times with bulk LM was higher than that of ink.

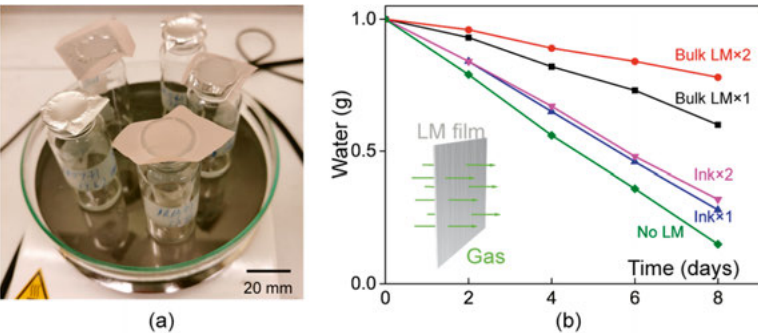


Figure 34. Gas permeability test. (a) A photo of the gas permeability set-up. (b) The water loss of different ways of deposition.

With a shadow mask, the LM line can be patterned on a wavy and rough surface in the micro-scale due to the excellent pass-through ability, as shown in Figure 35. The micrographs show that the high variations were similar to the area without patterning, indicating that the LM was conformally patterned.

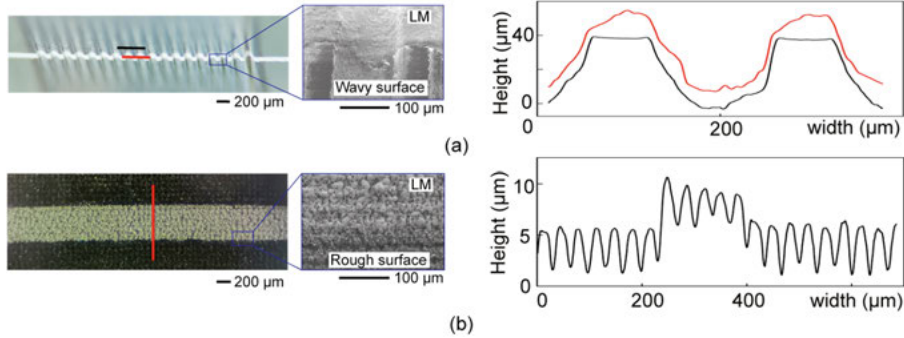


Figure 35. (a) Pattern on wavy surface. The diagram describes the height variation with and without LM. (b) Pattern on rough surface. The diagram is the height along the blue line in micrograph.

2.4.4 Microscale deposition based lift-off patterning

The top right micrograph in Figure 36a exhibits a group of LM lines with 20, 25, 30, and 35 μm width, and the diagram draws each cross-section of these lines. The top left micrograph shows a LED lighted with a 20 μm wide LM line, and the insert presents the line uniformity. To illustrate the capability of patterning interconnects for more complex circuits, circular and rectangle mazes were patterned in Figure 36b. A 15-pixel LED matrix (Figure 37c) was fabricated in $3 \times 5 \text{ mm}^2$ to manifest the possibilities in integrated electronics. The stretchable electronics could remain working when being curled, stretched, or twisted. The bottom left exhibits the patterned line for this device. A single-chip microcomputer (SCM) controlled the display of numbers and letters through 16 pairs of copper-LM interfaces.

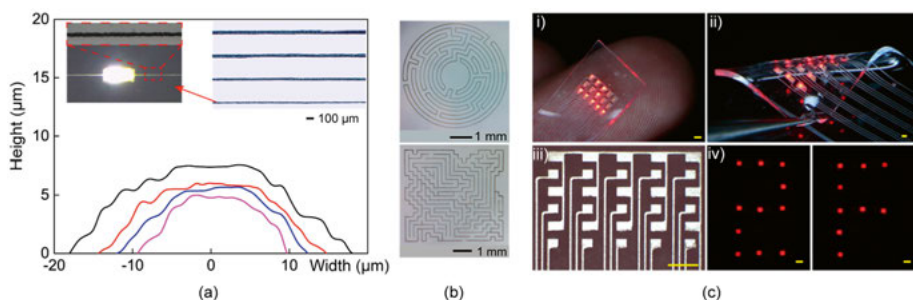


Figure 36. Capability verification and performance characterization. (a) The cross-section of LM lines with widths 20, 25, 30 and 35 μm from bottom to top, respectively. The broken line is 15 μm , which is the limit of resolution of the mask. Top left is a lightened LED with 20 μm width of line. (b) Fine circular and rectangle maze. (c) A lit 0201 LED matrix, i) the 3 \times 5 LED lighted by a control module on a fingertip, ii) works in twist state, iii) printing circuit, iv) digital controlled display with “2” and “F”. The scale bar indicates 1 mm.

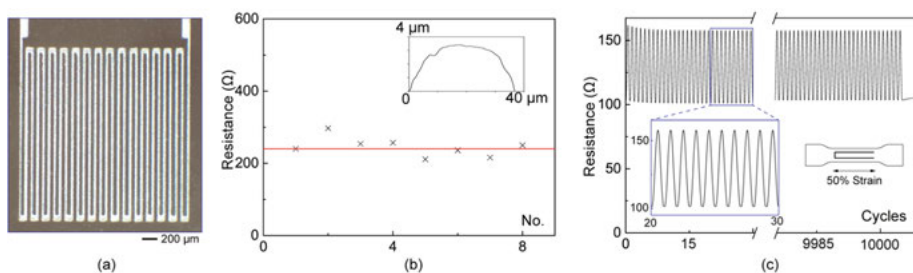


Figure 37. Repeatability and stability test. (a) A serpentine circuit, each with 9 cm length in a 3 \times 3 mm² area. (b) The measured resistances of eight serpentine circuits, the red line indicated the theoretical resistance based on the pure LM resistivity and the measured cross-section, inset was the measured average cross-section. (c) Stability of a fabricated strain gauge.

As the ink has no large droplets, this effectively eliminated the blocking of mask patterns with feature sizes in the tens of microns, leading to high yield at high-resolution LM patterning. A number of meandering lines with a length of 9 cm (3 mm \times 30) length were fabricated on a 3 \times 3 mm² area (Figure 37a). The zoomed micrograph presents their morphology, which exhibits good uniformity and reflects the depositing precision. As shown in Figure 37b, the chart is the measured average cross-section, and the red line is the calculated resistance when assuming its resistivity is equal to the pure LM. We found that each line had a resistance very close to this value, and the variation ratio about 10%. The results show that the LM line had an electrical resistivity comparable to that of bulk LM. It implies high quality, precise, and repeatable patterning and reflects the good coalescence and merging of nano/micro particles. A strain sensor was fabricated to test the electrical stability by strain cycling with a dynamic tensile system (E1000, Instron, USA). As shown in

Figure 37c, there was no noticeable resistance change even after 10,000 cycles with a 50% strain.

2.5 Transfer printing techniques

2.5.1 Stamp printing

It is known that the water is repelled by the lotus leave but can spread out on many metal surfaces. Their considerable difference in the contact angle (CA) can explain this phenomenon. Similarly, the LM contact angle is varied much with different surfaces. Researchers have introduced a selective printing technique based on the copper lithography technique [49], where copper is LM-philic (low contact angle), but the rest of the surface is LM-phobic (high contact angle). After pouring LM over the surface, only the copper pattern can hold it. On the contrary, in this work, we proposed an approach to treat the surrounding materials to reduce their wettability with LM so that only the non-treated area can hold LM.

According to Cassie's law, the contact angle could be tuned by the contact area with the substrate, and it is related to the surface roughness. In this study, the surface roughness was directly modified by a UV-laser. As shown in Figure 38a, micro/nanostructures on the treated surface can attract air effectively in the gaps, which decreases the effective contact area between the LM oxide layer and treated surface, further preventing liquid alloy from being pinned on the treated surface. The surface morphology can be tuned by the UV laser, scanning speed, scanning space, and power. We produced a group of surfaces with roughness 8.0, 4.5, 3.0, and 0.8 μm for the study.

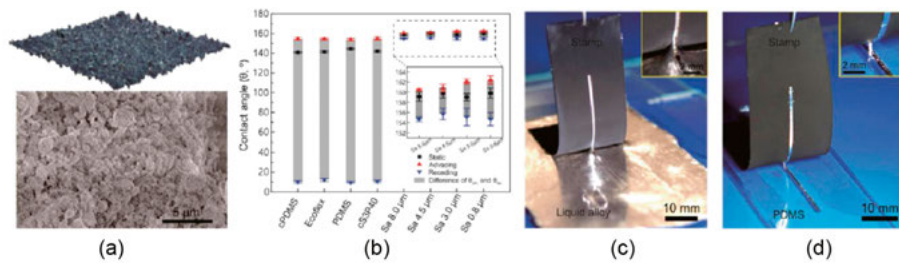


Figure 38. Surface selective modification for LM patterning. (a) SEM image of laser ablated surface. (b) Contact angles of LM droplet on different surfaces. (c) Selectively sticking LM from bulk. (d) Stamp transfer printing.

According to the classical definition of super-hydrophobicity, the measured static contact angle should be larger than 150° . In particular, high-quality super-hydrophobicity often means small variation between advancing and receding contact angles. Hence, we measured static, advancing, and receding contact angles of liquid alloy on the treated surfaces. The static contact angles

of UV-treated carbon-doped PDMS (cPDMS) ($\sim 160^\circ$) with different roughness (8.0, 4.5, 3.0, and 0.8 μm) are larger than that ($\sim 144^\circ$) of untreated surfaces (cPDMS, Ecoflex, PDMS, and cS3PDMS). Note that the surfaces with/without laser treatment show very similar behaviour, owing to the influence from naturally formed oxide layer. Huge differences appear in the variation of advancing and receding contact angles by comparing the surface with/without laser treatment. In particular, the differences of advancing angle and receding angle for UV-treated surfaces (within 8°) are significantly smaller than that (over 140°) for untreated surfaces, which refers to the fact that liquid alloy can easily be removed away from rough surfaces but will be pinned to the untreated smooth surfaces.

As shown in Figure 38c, the centre non-treated area can draw LM and separate it from the bulk. This soft substance could be either a substrate for patterning or a stamp to transfer printing LM onto the target substrate since the oxide is sticky to many soft substrates.

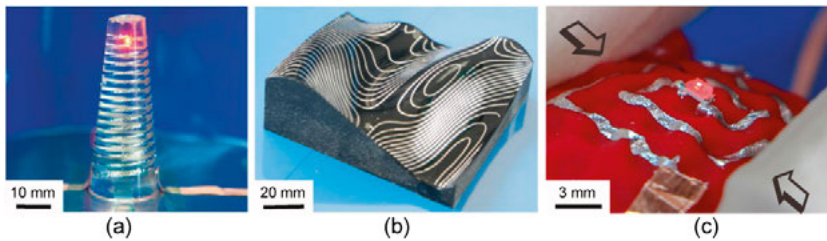


Figure 39. Patterns on 3D structure. (a) Spatial line on a cone. (b) Contour lines on 3D complex surface. (c) Liquid alloy circuit on a three-dimensional non-developable complex surface.

By rolling the cone on stamp with a preformed planar line, a spatial line was patterned on a cone surface. Due to the existence of focus depth, a 3D cPDMS replica (Figure 39b) can be treated by laser, and the remaining non-treated contour line is LM-phobic. Thus, after directly contact with LM, this contour line was patterned. Due to the compliance of silicones stamp, our printing technique can conformally transfer print liquid metal to both stiff and soft substrates, without introducing a dedicated 3D printer or advanced equipment. A liquid alloy circuit is printed on a silicone-replicated strawberry (Figure 39c), which has a non-developable surface and pits. Furthermore, coupling the stamp to a robot arm, automatically printing LM was demonstrated.

2.5.2 Hydroprinting

PVA is not only a material for lift-off patterning, but also as a medium for transferring LM from a planar surface to 3-D object. With the PVA changing from the solid film, swollen gel to the dissolved solution, it can carry, conformally transfer and fix the planar LM circuit onto the 3-D surface. Even the

surface is fragile, delicate, and non-developable. The fabrication process is illustrated in Figure 40.

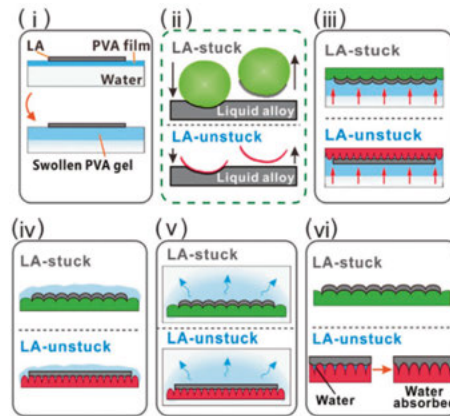


Figure 40. Fabricating process of hydroprinting LM pattern.

First, a PVA film with a pre-fabricated LM circuit is placed on the water surface. The target object is aligned toward the LM circuit and dipped into the water until the PVA becomes a swollen gel. In this step, the PVA gel is transferred and attached to the target object due to the surface tension and hydrostatic pressure. After drying, the whole structure is immersed in water and drying again to remove the residual PVA. With this process, different types of plants surface, which are LM-phobic, could be conformally patterned.

As shown in Figure 41a, line arrays with varying width and space were hydroprinted on the silicone hemisphere. A line as narrow as $70\ \mu\text{m}$ was achieved. Such resolution depends on the machining accuracy of the predefined patterning techniques. Furthermore, our process can also be applied to a curvature-discontinuous surface. For instance, a helical, high-fidelity LM-LED circuit was printed on a 3D non-developable surface with corrugated wrinkles, including positive and negative Gaussian curvatures (Figure 41b).

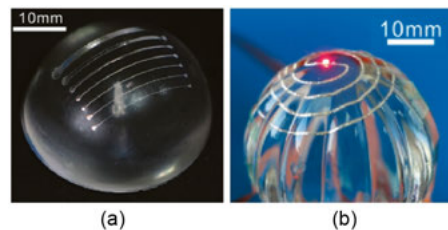


Figure 41. Hydroprinting LM based electronics on 3-D scenario. (a) Arrays of varied LM line on a hemisphere. (b) A helical LM circuit on a curvature-discontinuous glass sphere. A sinuous length sensor patterned on the rose petal (c) and on a living bean sprout seedling (d).

3 Applying a conformal and gentle contact to living beings

3.1 Epidermal Strain Sensor

An epidermal strain sensor is an important part of skin-like electronics systems. When stretched, the LM that is encapsulated in the thin elastomer will follow the stretched elastomer and its channels. Thus, a changed electrical resistance will reflect the changed geometry of the conductor. A bidirectional sensor consisting of two strain sensors orthogonally aligned is shown in Figure 42a. The measured resistance shows that the strain in X-axis is larger than the Y-axis with the elbow movement. This was because the sensor's X-axis had a more acute angle with the moving direction of the elbow.

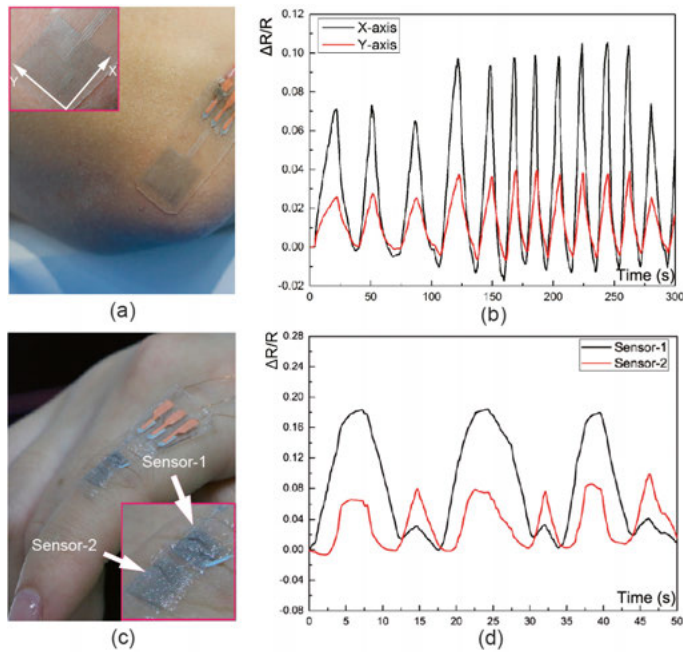


Figure 42. Strain sensors for skin movement monitoring. (a) A bidirectional strain sensor adhered to an elbow (inset), (b) and its perceived signal. (c) An epidermal strain sensor adhered to an index finger, (d) and its perceived signal.

To accurately monitor the skin movement, especially the skin that wrinkles on a joint, an epidermal strain sensor, is thin, flexible and stretchable, and sticky, was developed. As previously shown in Table 2, S3-PDMS and Ecoflex has similar stretchability with our skin. With masked deposition, we fabricated a self-sticking epidermal strain sensor ($\sim 80\text{ }\mu\text{m}$ in thick) with two parallel-aligned local strain sensors. It could monitor fine strain variations as well as overall strain in local areas ($< 5\times 5\text{ mm}^2$). The sensor was conformably adhered to an index finger when the finger skin was in a natural relaxed state. One strain sensor (Sensor 1) was placed exactly above the joint and the other (Sensor 2) on the side toward the fingertip (Figure 42c). The adhesion of S3-PDMS and similar stiffness and stretchability make the sensor follow the local fine skin movements accurately. The diagram (Figure 42d) shows the resistance fluctuation during the bending, which has the same trend of skin since Sensor 1 has more and deeper wrinkles. To assure the validity of our monitoring, the comparison of the finger bending with or without mounted sensors showed that no noticeable movement distortion was observed during the whole bending circle.

A single finger bending cycle was extracted (Figure 43) to find the relationship between resistance change and finger skin movement. As mentioned previously, the sensor conformably adhered to the finger when the finger skin was flat (State 0, Figure 43a). Here, the Sensor 1 area had shallow wrinkles, and the liquid alloy circuit was in a slightly wavy distribution. When the finger moved toward a straight state (State 1), where deep wrinkle trenches gradually formed due to the compression of the skin and finally led to a highly narrow distribution of the liquid alloy inside the sensor, a strong peak occurred when bending from State 0 to 1 (Figure 43c). When the finger bent back to the flat state (State 2), where the wrinkles became flattened, the signal significantly decreased, changing from State 1 to State 2. Continuous bending of the joint to its maximal state (State 3), the skin was further stretched, and the wrinkles disappeared, where liquid alloy was elongated to a narrower line. An apparent resistance increase was appeared when moving from State 2 to 3, and another peak signal appeared at maximum bending. Sensor 2 also experienced a synchronous fluctuation of resistance change along the bending process (not described here in detail). Finally, three pairs of sensors worked simultaneously on different fingers to record the grasping process.

According to our observations, when the skin is either wrinkled or elongated, the resistance increases. A single LM line was embedded in a thin elastomer structure to experimentally study the relationship between the resistance change and the wrinkle formation. The micrographs in the insets (Figure 43d), show that when the sample is bent, the microchannel with its LM becomes narrow.

Assuming a straight conductor at length L with a uniform rectangular cross-section with width W and height H , its electrical resistance R is proportional

to $qL/(WH)$, where q is the resistivity of liquid metal. According to our simulation, any bending started from a uniform straight will increase its electrical resistance. Specifically, when a wavy distribution forms, a higher curvature leads to a higher resistance, as shown in Figure 44, which matches our experimental observation in Figure 43d. In addition, from a geometric perspective, State 0 and State 2 should be the same. The hysteresis of polymer viscoelasticity may cause the difference in resistance. A more detailed test in one cycle was conducted, which exhibited minor hysteresis when the sensor was stretched and released (Figure 45).

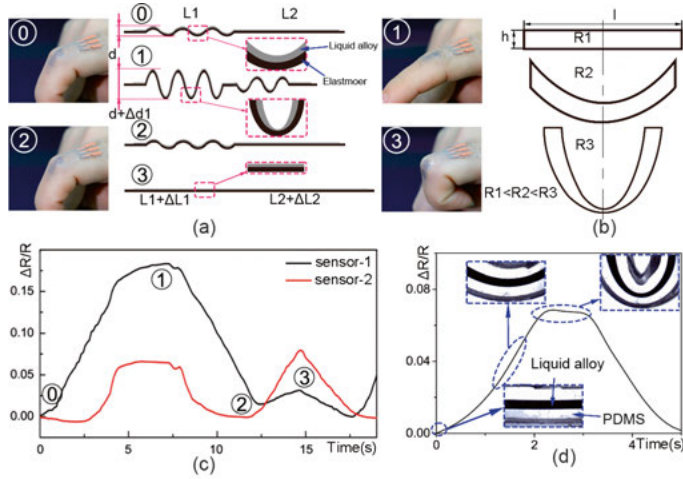


Figure 43. The detail of wrinkle skin movement. (a) Photos and illustrations of each bending stage. (b) Explanation of the resistance changing from the lateral view of microchannel for the bending at the minimum (R1), middle (R2), and maximum (R3) state. (c) Signal change in a single cycle. (d) The resistance change of strain sensor with bending induced by a single bending, and the zoomed lateral view of micrographs of the liquid alloy deformation in the microchannel.

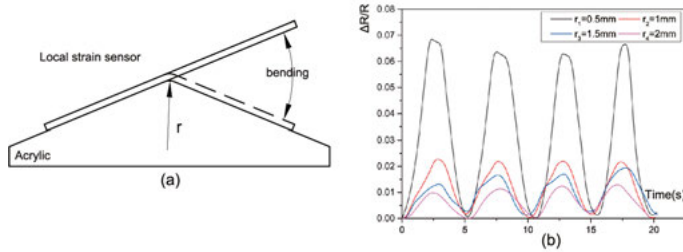


Figure 44. Bending curvature impact on resistance. (a) The bending curvature test, (b) the resistance change with different bending curvature. The curvature was guaranteed with a 6 mm thickness acrylic board that was shaped in different radius but same arc length by a laser cutting plotter. One side of the sensor one side was attached on an acrylic foil, and the other side was bent from straight state to the surface.

Due to the polymer hysteresis, we test the signal hysteresis. Each strain sensor was stretched from 0 to 50% and then released to 0 by a dynamic tensile system (E1000, Instron, USA).

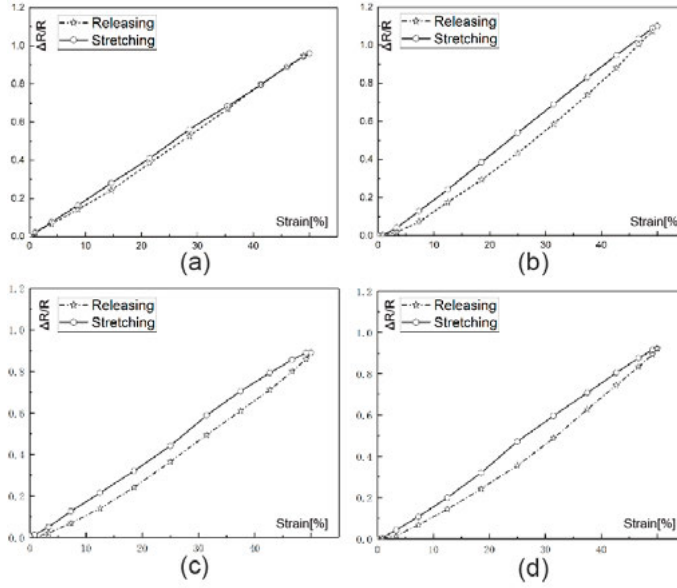


Figure 45. The hysteresis test. The resistance changes of X-axis (a) and Y-axis (b) direction of bidirectional sensor versus strain. The resistance change of sensor 1 (c), and sensor 2 (d) of local sensor versus strain.

3.2 Compliant micro-heater

Epidermal skin-like strain sensor can perceive augmented signal for monitoring the skin movement. It also is able to provide accurately thermal activation. Localized ectopic expression of enteroendocrine (ee) cells [91-100] in fruit flies could be a model for studying human intestinal diseases. It could provide exclusive information on the ee-secreted intestinal hormones [101-103], which is important for studying many intestinal diseases like the inflammatory bowel disease [104-105].

Due to the non-invasive feature, thermal activation [106, 107] is an option to specific ectopic expression of ee cells in intestinal cells of *Drosophila*. By locally controlling the temperature of flies' abdomen, the genetic cassettes will be only thermally activated in the intestinal epithelium. However, the adult *Drosophila* is tiny (1 mm in diameter and 2 mm in length) and its abdomen cuticula is fragile and with an oval surface. To uniformly and precisely provide the heating on abdomen, a skin-like microheater with relative high-density heating elements is needed to conformally attach over the abdomen. Otherwise, the *Drosophila* would be point heated or global heated, losing the

localized ectopic expression. Moreover, negligible physical disturbance is needed to keep the small and delicate organisms alive during the entire heating process, which is necessary for ectopic expression.

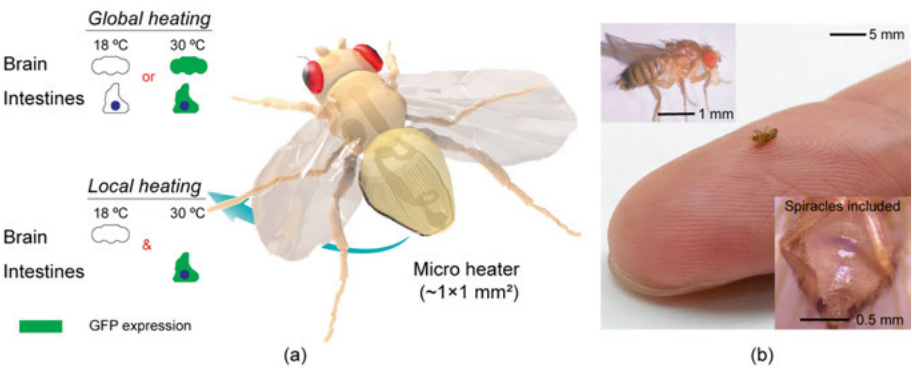


Figure 46. Schematic illustration of spatiotemporal-specific gene expression system. (a) The thermal activation conditions. (b) Photos of *Drosophila*, the insets show its detail.

Based on these demands, a skin-like high-resolution micro-heater was fabricated (Figure 47a). The whole area is about 1×1 mm², was compliantly attached to the abdomen of a tiny fly. From the high-resolution infrared camera, we could find that the local temperature on the abdomen is 30 °C, and the head is 18 °C. The detail about the temperature rising process is extracted (Figure 47c), the result indicates that the temperature is stable and accurate. We have checked that the temperature remains stable even after 12 hours.

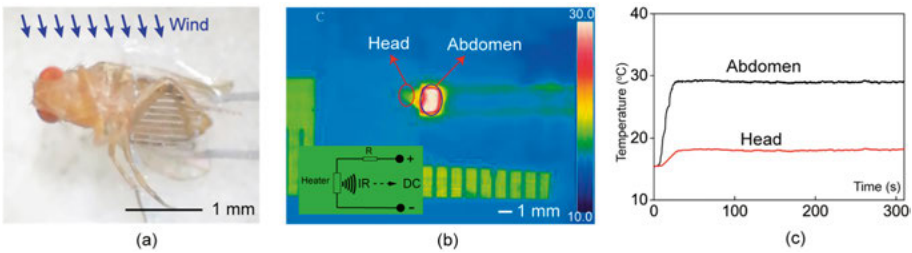


Figure 47. Temperature regulation system. (a) The soft skin-like micro-heater attached on the abdomen. (b) Infrared image of temperature detection, the insets express the control mechanism. (c) Heating process.

With skin-like microheater, most *ee* cells (*pros*⁺ cells, red) at were labelled with green fluorescence protein (*GFP*) co-localization, while *GFP* is undetectable in the same fly brain (Figure 48). Only culturing files in 18 °C or 30 °C, never show this expression difference.

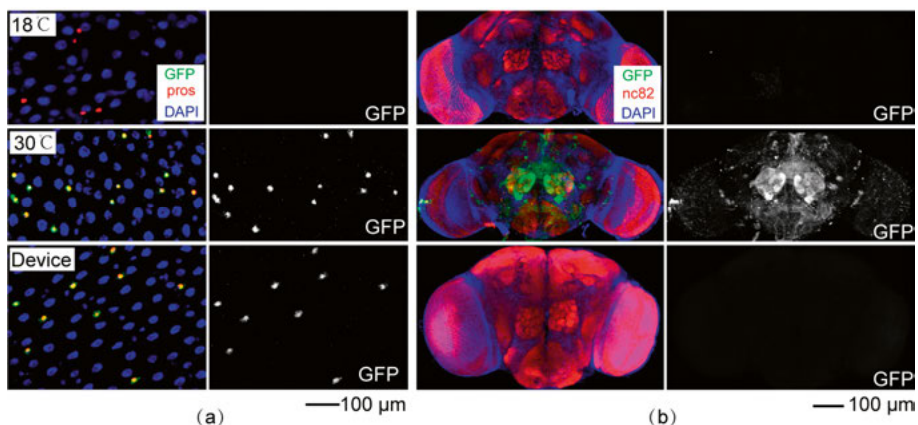


Figure 48. Demonstration of local thermal activation of ectopic expression in entero-endocrine cells. (a) Immunostaining analysis of GFP expression driven by *pros^{ts}* in intestines at 18 °C (upper), 30 °C (middle) and device (bottom). Here and in all images, green indicates GFP; blue indicates 4',6-diamidino-2-phenylindole (DAPI). GFP was expressed in ee cells (*pros*-positive, red) in 30 °C (background or device generated temperature) but not at 18 °C. (b) Immunostaining analysis of GFP expression driven by *pros^{ts}* in brains at 18 °C (upper), 30 °C (middle) and device (bottom). GFP was expressed in neurons (*nc82*-positive, red) at 30 °C and but not at 18 °C or with the micro-heater.

As shown in Figure 49, there was no cell apoptosis (cleaved caspase-3 positive) in the gut epithelium when flies were raised at 18 °C or 30 °C. Besides, when we heat *pros^{ts}>GFP* flies with the micro-heater, there was no apoptosis cell in the gut epithelium.

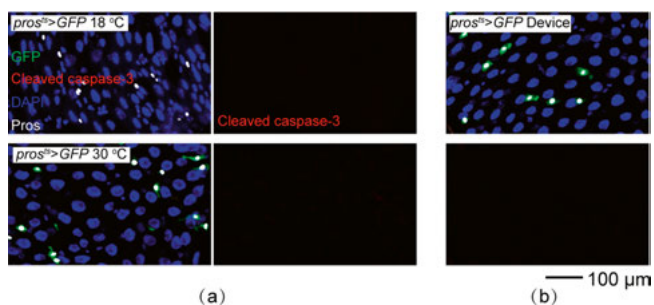


Figure 49. The heating effect on apoptosis. Immunostaining analysis of cleaved caspase-3, the apoptosis marker, expression in gut epithelium when flies were raised at a global temperature of 18 °C and 30 °C (a), or locally at 30 °C (b), using the heater device.

Since the abdomen, with many pores for breathing, was covered for 12 hours, we also tested the heater permeability. The device had the same LM density as the heater (Figure 50). We found that the gas permeability was reduced a

small degree after embedding LM. The thick device's weight loss implies that keeping the device thin is an effective way to maintain gas permeability.

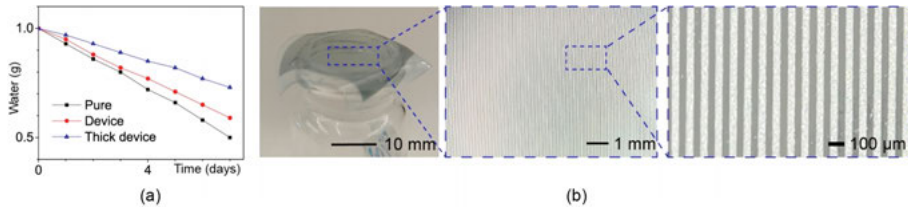


Figure 50. (a) Gas permeability test of the device. (b) The patch sealed on vial. The bottom and top layer of heater and device were PDMS (Sylgard 184) with 40 μm and Ecoflex(00-30) with 40 μm . The thick device had double the thickness. The open of the vial is 18 mm in diameter and is fully covered by the pattern as the LM patterned area is 25 mm \times 25 mm. The patterned device was glued to vial with silicone glue.

LM patterned thin, compliant, and lightweight micro-heater with different designs will allow for labelling and exploring many kinds of exclusive functions in *Drosophila* tissue. For example, ee cells only account for 5-10% of midgut epithelium cells in *Drosophila*. More than 90% cells of gut epithelium cells are enterocyte cells (ECs) [108]. ECs play essential roles in digestion and absorbing nutrition, [109] regulating host immunity [110], and gut homeostasis [104, 109, 111]. The widely used EC “specific driver” *Myo1A*-Gal4 is also expressed in the *Drosophila* brains [112]. Just like in localized ee cells manipulation, the compliant printed heater combined with *Myo1A*^{ts}, can be used to investigate the function of ECs more accurately by avoiding cross-talk from genes expressed in the brains. On the other hand, such compliant printed heaters should be feasible for the abdomen organs. For example, combined with a neuron-specific driver, they can achieve better localization to the fly head, which would be an elegant tool for neurobiology studies.

3.3 Plants monitoring and manipulation

The surface of the plant is usually fragile, vulnerable, and has a complex surface, which makes monitoring its physiological signals challenging. Hydro printing of LM to this surface is an option to solve this problem.

When the functional LM circuit was transferred to a rose petal (Figure 51), we found that it could stably remain on the surface. After dehydration, the circuit still worked quite well. To monitor the physiological signal of plants, we transferred an LM strain sensor to the surface for perceiving the water content. As the petals dehydrated, the LM became thicker and shorter, reducing the resistance.

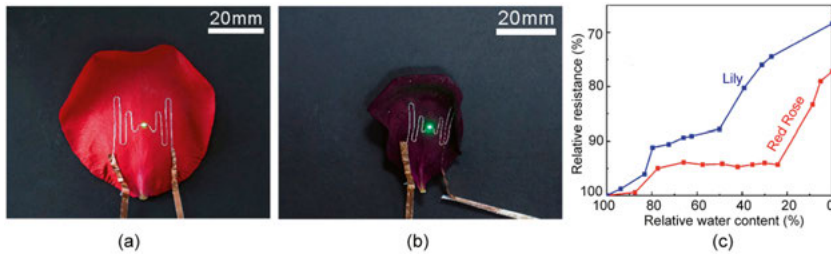


Figure 51. A LED was lit both on the fresh (a) and withered (b) rose petal. (c) Water loss of lily petal and red rose versus resistance variation.

When the LM was transfer printed on the sprout (Figure 52), it could be used to monitor the length during its growth. Due to the stable fixing on the sprout, the LM volume is constant. As it grew, the sprout was extended, which would stretch the LM sensor, making it narrower and longer, increasing resistance. Due to the phototropism of the bean sprout, we could manipulate its growth orientation by adjusting the light-emitting angle. In addition, we have controlled the bending angle changing from 0° to 180° as compared to that of the pristine control. More interesting, two LEDs were mounted on the two sides of the sprouts, which are lighted by transfer printed LM circuit. By sequentially changing the light emission in a black box, we could manipulate the growing orientation so that it was growing through a ladder, Figure 52c.

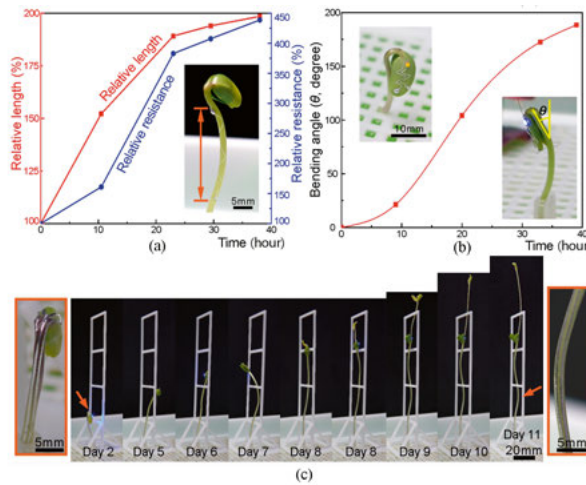


Figure 52. The sprout growth monitoring and manipulation. (a) Length monitoring. (b) Bending versus time under LED illumination. (c) Manipulating sprout to climb a ladder.

4. Summary of papers

Paper I. High-Performance Liquid Alloy Patterning of Epidermal Strain Sensors for Local Fine Skin Movement Monitoring

This paper proposed a novel thin sacrificial mask, which provided lift-off at high resolution, enabling the fabrication of an LM based high-resolution skin-like sensor. The sacrificial mask was made of water dissolvable PVA and patterned by a nanosecond UV laser, so that the resolution, density, and complexity could reach a high fidelity.

This paper introduces an environmental friendly technique to produce the sacrificial mask by introducing a water dissoluble mask together with a UV laser processing technique. By adding pigments in pure PVA, it got a high UV light absorption. Due to the laser spot Gaussian energy distribution, after the one-time transfer, the fabricated side wall was inverted with a sharp edge at its top,, which plays a critical role during lift-off. It eased the separation of the LM deposited on the target substrate and on top of the mask. Thereafter, the sacrificial mask was easily removed without damage to the needed pattern by dissolving it in water. With this technique, the smallest width of the liquid metal line was down to 30 μm , and the narrowest space between lines was down to 40 μm . In addition, isolated patterns were demonstrated, which are necessary for most electronics circuits.

Finally, a thin and soft skin-like strain sensor was fabricated and conformally mounted on the finger joint to monitor the movements of the wrinkled skin. From the data, the monitor system could display the folding and unfolding of wrinkles during bending.

Paper II. Sandwiched Polyethylene Shrink Film Masking with Tunable Resolution and Shape for Liquid Alloy Patterning

This paper proposed a shrinkable mask, which could shrink from original large size to a much lower size with different but predictable shape. The mask is made of shrink film and produced by a low-cost cut plotter. After shrinking, the shrunken mask could have three times higher resolution (shrinking from 100 μm to 34 μm), and even could be used on a non-planar surface.

Like other mask-based processes, the patterning is often constrained by mask fabrication, and the cost increases drastically with increased resolution. In this paper, we demonstrated a facile technique to fabricate a mask with tuneable and predictable resolution and shape in tens of microns by introducing a thermal shrink polymer film, a mechanical cutting plotter, and a low-cost ordinary oven that are highly accessible.

During manufacturing, the original entangled polymer chains have been orientated stretched. With the polymer chain relaxing, shrink polymer film can shrink to a specific ratio after heating. This paper presented a sandwich structure to make sure the synchronization of shrinking. It contains two layers of shrink film, the top patterned layer and bottom un-patterned layer, with an organic agent in between. This sandwiched structure is critical to assure the whole pattern shrinking homogeneously even when the pattern is complex and has isolated structure. The mask's final resolution and shape can be tuned based on the shrink polymer film's orientation and other operational parameters of the technique like heating time and temperature. After shrinkage, the width of the patterned liquid alloy lines and space in-between could be tuned to less than one-third of the original cut pattern, to about 35 μm and 60 μm , respectively, according to requirements. Furthermore, conformal masking were exhibited on cylindrical and spherical surfaces.

Paper III. Liquid metal microscale deposition enabled high resolution and density epidermal microheater for localized ectopic expression in *Drosophila*

This paper proposed a strategy to deposit LM with micro/nano particles. Spray-driven collision of particles is introduced to rupture and merge the micron/submicron particles, which have the typical core-shell structure and an electrically insulating shell. By integrating this mechanism into the LM masked deposition, the repeatability and manufacturing success rate are largely enhanced. Therefore, it is possible to pattern micro-heater for localized (1 mm^2) ectopic expression in *Drosophila*, which requires high-density LM pattern at high resolution.

Localized ectopic expression of enteroendocrine cells in *Drosophila Melanogaster* *in vivo* can make a better model for studying intestinal diseases, *e.g.* inflammatory bowel disease. One way is local thermal activation, but this is challenging on small and delicate organisms, *e.g.*, tiny arachnids or insects. Soft and thin micro-heaters with encapsulated liquid metal (LM) should hold a high potential for such localized studies, but the patterning technology was not well developed for making them.

In this study, we have investigated the mechanism of the sintering of LM core-shell micron/submicron particles by managing the parameters of spraying, SEM imaging, and high-speed camera. Compare to traditional spraying of bulk LM, spraying an ink with micron/submicron LM particles brings stable, precise, and reproducible patterning. Moreover, LM could be conformal printed on wavy or rough surfaces, and the deposited sheet was gas permeable.

Applying such a fabricated thin, compliant, and lightweight micro-heater on the abdomen of a living fly with a suitable genotype, localized ectopic expression of enteroendocrine cells also was successfully demonstrated by controlling the temperature of the abdomen to $30\text{ }^{\circ}\text{C}$ while keeping its brain at the ambient temperature $18\text{ }^{\circ}\text{C}$. In addition, there was no cell apoptosis in the gut epithelium when flies were raised to $30\text{ }^{\circ}\text{C}$.

Paper IV. High Fidelity Conformal Printing of 3D Liquid Alloy Circuits for Soft Electronics

In this paper, we made a flexible stamp in which patterns can be transfer printed when the stamp comes to contact with LM. This pattern can be directly integrated with electronics or transferred onto target substrates as the traditional stamping process. Due to the flexibility of the plate, the pattern can be transferred to the 3-D surface like pad printing.

Although various printing techniques have been demonstrated, techniques using the mature flexography printing to pattern liquid metal circuits in a highly efficient way and print on 3D surface are not yet available.

In this work, by selectively modifying the morphology of a material matrix with laser, we created a surface that has different wettability with LM. Only the untreated area has good wettability with LM, which is confirmed by the contact angle measurement. The difference is caused by the roughness of the surface, which can be tuned by the parameters of the laser. Thus, by contacting the plate with liquid alloy and then transferring the liquid alloy onto a target substrate, we demonstrate a way of flexography printing of liquid circuits on diverse substrates. Furthermore, thanks to the excellent compliance of the silicone plate, the circuits can be directly printed onto a complex 3D surface conformably.

Paper V. Hydroprinted Liquid-Alloy-Based Morphing Electronics for Fast-Growing/Tender Plants: From Physiology Monitoring to Habit Manipulation

PVA film has been previously developed to fabricate a sacrificial mask. This paper proposed a technique to transferring the LM pattern from a planar surface to a 3D surface with a medium PVA film.

Although emerging epidermal electronics that can conveniently acquire vital signals of living organisms, it is a significant challenge to adapt such devices for plants, because they are fragile and usually have complex surfaces that can change significantly during rapid growth. A gentle fabrication process is critical in order to employ compliant electronic systems to adapt to this highly dynamic situation.

In this work, PVA film was introduced firstly as a carrier to support planar LM pattern, and afterward as a swollen gel to smoothly and conformally transfer pattern on the target substrate, and finally disappeared to make the LM pattern still flexible and stretchable. In detail, the accuracy of transferring and the contact angle change after wetting has been investigated. Furthermore, a sensor can be patterned on a fragile and delicate rose petal or a living bean sprout seedling, to record the physiology like withering or growing process.

4. Conclusion

In this thesis, masked deposition of LM is widely discussed with significant development in mask fabrication and LM deposition, targeting LM-based skin-like soft, thin, and high-resolution skin-like electronics. It can provide a soft and gentle contact to living beings for information exchanging and stimulation. On the other hand, two transferring printing techniques are introduced, which could transfer printing skin-like electronics to 3D surface, demonstrating the possibility of interfacing with complex 3D soft tissue.

A sacrificial mask is an inseparable element when the patterning resolution reaches high level. The first work demonstrated a thin, flexible, and high-resolution sacrificial mask, which is capable of fabricating high-resolution skin-like electronics for detecting local fine skin movement. By combing a water dissolvable PVA film and a nanosecond UV laser, the needed sacrificial mask can be obtained. The mask has demonstrated the ability to ease the lift-off process, contributing to high resolution and complex patterning fabrication. Finally, two types of fabricated skin-like strain sensors successfully obtain the skin movement data demonstrate that the skin-like sensor, which consists of thin super-elastic material and its encapsulated stretchable conductor, can be a good combination for skin movement monitoring for athletes training or muscle rehabilitation. Furthermore, the whole process is highly efficient and well-controllable, making it has high potential for future industrial skin-like electronics automatically manufacturing.

By introducing a thermal shrink polymer film, the second paper presented a low-cost technique to fabricate a high-resolution planar or 3D conformal mask with shrink film for LM patterning. This technique is capable of shrinking original low resolution mask to high resolution, such as from width 100 μm or space 200 μm to 35 μm or 60 μm , respectively. This sandwiched structure can effectively assure the whole pattern shrinking homogeneously even when the pattern is complex and has isolated structure, which makes the shrinking process predictable.

The microscale deposition demonstrates a way to deposit a microscale thin (5 μm), smooth ($S_a=0.8$ μm) gas permeable LM film. During printing, the deposition process has a high pass-through capability, making this technique can conformally printing on the wavy or rough surface. Together with the sacrificial mask, this deposition technique is able to stably pass through a very narrow open due to the tiny and narrow distributed size, making it capable of

fabricating thin, high-resolution, and high-density LM-based skin-like microheater. Compared to airbrush pure LM, this technique is able to produce high yield and reproducible thin LM pattern with high-resolution, density, and precision properties simultaneously. The biological results demonstrated that this conformal skin-like microheater can locally thermal activate the abdomen, and proved that this technique is an excellent alternative for LM based skin-like electronics fabrication. This technique maybe extend to other printing method, such as selective wetting, laser ablation, and imprinting, since they all improve with thin and smooth LM film and may be applied where gas permeable conductive layers are needed.

To conclude, masked atomization and deposition of liquid metal is attractive since it is a batch process that can pattern highly dense and complex circuits on various elastomer substrates. This thesis has advanced this technique in mask and deposition, but it is far from enough and can be further optimized. One issue is that the damage or distortion might happen during the mask transferring process, especially when the resolution reaches a high level of complexity. This can be solved by mounting the mask on the target substrate directly, but a series of accompanied problems must be handled. Another issue is that the resolution is limited by laser spot, this might be addressed by intruding traditional lithographic techniques, such as photoetching, focused ions, or electron beam. This thesis has successfully demonstrated a technique to coalesce and merge micron/submicron LM particles, which is not only suitable for masked deposition but can be further extended to other techniques as transferring printing because of its depositing uniformity.

Flexography printing is engaging in the conventional industry. By tuning the wettability of liquid metal to substrates through a selective surface morphological modification, this thesis presented a flexography printing technique to transferring pattern liquid alloy circuits on both planar and 3D complex surfaces, and also have investigated the tuning mechanism and the relation between the wettability and surface morphological modification.

PVA film also can be a medium to transfer the LM pattern from a 2D surface to a 3D surface with a PVA film. A gentle hydroprinting technique to pattern compliant electronic on plants that could sense physiological signals and even function as a biohybrid to determine plant behaviour on demand. Functionally, the conformal architecture can monitor leaf moisture content and length and manipulate leaf and bean sprout orientation.

In summary, targeting exploring LM patterning techniques, several LM-based compliant electronics have been fabricated, and their potentials in skin-based electronics also have been demonstrated. However, this is far from enough to introduce skin electronics to the market, as energy supply, peripherals, and digital communication should be considered and integrated to advance further.

5. Acknowledgements

I do believe that I will never forget the journey as a Ph.D. student at the Division of Microsystems Technology. I have learned a lot during this period, not only scientific knowledge and skills, but also life experience. In the future, when people ask me about this journey, I will be proud to tell them all the wonderful people and things I met here. I want to take this opportunity to express my gratitude to all of them.

First of all, my supervisors Klas and Zhigang. Thank you for offering me the opportunity to become a Ph.D. student. Without your offer, I would be somewhere else, doing something else and living another type of life. I am lucky to have both of them as supervisors, and their different expertise is an excellent combination to help me look into the study and experiment from different perspectives. Thank you, Zhigang. I appreciate the discussion you have contributed to guide my research and experiment. I learned many things in academics about building a concept and making thing more attractive from scientific perspective. Thank you, Klas. I appreciate the support you have provided for my life in Sweden. And you have a broad range of knowledge in microsystem technology. I can always get a hint from you to solve whatever problem I have met in the research and experiment. Also, your expertise about transferring scientific results to an industrial product or application always motivates me to make our techniques more realistic and valuable. Again, I am grateful to have both as my supervisors. Thanks for all your supports.

Many thanks to the members of the group Soft Intelligence at Huazhong University of Science and Technology. Shuo and Jiajun, we have been a team and struggled a lot about advancing the experiments and research at the beginning, but we have mutual achievement now. I enjoy our jointed striving time and wish you a promising future. Wenci, we made a paper published in only about four months, which is a pretty cool thing. I wish you an exciting academic journey at National University of Singapore. Zenghui, I dare to say you must have seen fruit flies in your dream during the intensive experiment days, at least I had. I was truly delighted when I heard that you got the desired position in a giant company, and I wish you a successful career. Fen Li, thanks for your great help on the experiments. I wish you a pleasant academic journey in Germany.

Sincere thanks to the SINTEC group members, Jan and Klara. You have offered a lot of help, including purchasing experimental stuff, introducing the

materials and equipment, lab rules, *etc.* I also have learned a lot about the techniques to fabricate soft and stretchable electronics from you. I am sure we will have jointed results in the near future. And Klara, I wish you a successful career in the new company. Seunghee, Filip and Jing, although you just came here lately, but we have many fruitful discussions. Oscar, you are quite a fast learner, thanks for your helping on the glue.

I would like to thank you for all the help and company from the MST and EMBLA. Zhenhua, thanks for your warm help in daily life. Without your help, I would have spent much time and effort looking for accommodation and familiar with life. Qian and Yuan, thanks for your help in daily life. Federic, thank you for organizing a particular party for me. Hugo, thanks for your suggestions and help in my experiments. Javier, Simon, Karolina, Sarah, Ana Maria, Farnaz, Abdul, Gabriel, Atena, Lena, Laurent, Anton, Lulu, Hanlu, Maja, thanks for your help in the lab, and I am really enjoy the time with you.

I sincerely acknowledge all the collaborators. Hao and Anders, thanks for your help on the cochlea implant experiment. Robin and Pramod, thanks for your help on the antenna test. Alessandro, thanks for your patience on guiding me to design the printed circuit board. Gustaf, thanks for your help on the aerosol and pick & place machine.

I have met many Chinese friends here, Qitao, Huan, Zhuyuan, Xueying, Zhouyuan, Hongyi, Yuzhou, Chenyu, Renbin, Pei, Shuangshuang, Yintao, Zheqiang, thanks for your help, I appreciate your company.

Last but most important, thanks to my family. My lovely wife, kids, parents, and parents-in-law, I could not have made this journey without your patiently support. I want to express my deepest gratitude to you. My kids, I am sorry that I have not spent enough time accompanying you and playing games with you.

Ph.D. journey is tough, but I am lucky to have all of you around. You never know, maybe just because of your casual smile, my frustration disappeared and I became an energetic researcher again.

Thank you all!

Bei Wang

Nov. 22th, 2021

The Ångström Laboratory, Uppsala, Sweden

Reference

- [1] Vatier C, Poitou C, Clement K. (2014) Evaluation of Visceral Fat in Massive Obesity. *Nutrition in the Prevention and Treatment of Abdominal Obesity* 68-73
- [2] Chu B, Burnett W, Chung J W, Bao Z. (2017) Bring on the bodyNET. *Nature* **549** 328.
- [3] Kim D H, Lu N, Ma R, *et al.* (2011) Epidermal electronics. *Science* **333** 838.
- [4] Hammock M L, Chortos A, Tee B CK, *et al.* (2013) The Evolution of Electronic Skin: A Brief History, Design Considerations, and Recent Progress. *Adv. Mater.* **25** 5997-6038.
- [5] Rogers J A, Someya T, Huang Y. (2010) Materials and mechanics for stretchable electronics. *Science* **327** 1603-1607.
- [6] Trung T Q, Lee N E. (2016) Flexible and Stretchable Physical Sensor Integrated Platforms for Wearable Human-Activity Monitoring and Personal Healthcare. *Adv. Mater.* **28** 4338-4372.
- [7] Dagdeviren C, Su Y, Joe P, *et al.* (2014) Conformable amplified lead zirconate titanate sensors with enhanced piezoelectric response for cutaneous pressure monitoring *Nat. Commun.* **5** 4496.
- [8] Wang X, Gu Y, Xiong Z, Cui Z, Zhang T. Silk-Molded Flexible, Ultrasensitive, and Highly Stable Electronic Skin for Monitoring Human Physiological Signals *Adv. Mater.* **26** 1336-1342.
- [9] Kang D, Pikhitsa P V, Choi Y W, *et al.* (2014) Ultrasensitive mechanical crack-based sensor inspired by the spider sensory system. **516** 222.
- [10] Kwon K Y, Shin Y J, Shin J H, Jeong C, Jung Y H, Park B, Kim T. (2019) Stretchable, Patch-Type Calorie-Expenditure Measurement Device Based on Pop-Up Shaped Nanoscale Crack-Based Sensor. *Adv. Healthcare Mater.* **8** 1801593.
- [11] Yamada T, Hayamizu Y, Yamamoto Y, *et al.* (2011) A stretchable carbon nanotube strain sensor for human-motion detection. *Nat. Nanotechnol.* **6** 296-301.
- [12] Amjadi M, Pichitpajongkit A, Lee S, *et al.* (2014) Highly stretchable and sensitive strain sensor based on Silver nanowire-elastomer nanocomposite. *ACS Nano* **8** 5154-5163.
- [13] Muth J T, Vogt D M, Truby R L, *et al.* (2014) Embedded 3D printing of strain sensors within highly stretchable elastomers. *Adv. Mater.* **26** 6307-6312.
- [14] Cai G F, Wang J X, Qian K, *et al.* (2017) Extremely stretchable strain sensors based on conductive self-healing dynamic cross-links hydrogels for human-motion detection. *Adv Sci* **4** 1600190.
- [15] Xu S, Zhang Y H, Jia L, *et al.* (2014) Soft microfluidic assemblies of sensors, circuits, and radios for the skin. *Science* **344** 70-74.
- [16] Chung H U, Kim B H, Lee J Y, *et al.* (2019) Binodal, wireless epidermal electronic systems with in-sensor analytics for neonatal intensive care. *Science* **363** 947.
- [17] Huang Z, Hao Y, Li Y, *et al.* (2018) Three-dimensional integrated stretchable electronics. *Nat. Electron.* **1** 473.

- [18] Xu J, Wang S, Wang G N, *et al.* (2017) Highly stretchable polymer semiconductor films through the nanoconfinement effect. *Science* **355**, 59
- [19] Wang S, Xu J, Wang W, *et al.* (2018) Skin electronics from scalable fabrication of an intrinsically stretchable transistor array. *Nature* **555** 83.
- [20] Yang J C, Mun J, Kwon S Y, Park S, Bao Z, Park S. (2019) Electronic Skin: Recent Progress and Future Prospects for Skin-Attachable Devices for Health Monitoring, Robotics, and Prosthetics. *Adv. Mater.* **31** 1904765.
- [21] Dickey M D. (2017) Stretchable and Soft Electronics using Liquid Metals. *Adv. Mater.* **29** 1606425.
- [22] Wu H, Yang G, Zhu K, Liu S, Guo W, Jiang Z, Li Z. (2020) Materials, Devices, and Systems of On-Skin Electrodes for Electrophysiological Monitoring and Human-Machine Interfaces. *Adv. Sci.* 2001938
- [23] Lipomi D J, Vosgueritchian M, Tee B C K, Hellstrom S L, Lee J A, Fox C H, Bao Z. (2011) Skin-like pressure and strain sensors based on transparent elastic films of carbon nanotubes. *Nat. Nanotechnol.*, **6**, 788.
- [24] Wang Y, Zhu C, Pfattner R, *et al.* (2017) A highly stretchable, transparent, and conductive polymer. *Sci. Adv.* **3** e1602076.
- [25] Matsuhisa N, Inoue D, Zalar P, Jin H, Matsuba Y, Itoh A, Yokota T, Hashizume D, Someya T. (2017) Printable elastic conductors by in situ formation of silver nanoparticles from silver flakes. *Nat. Mater.* 2017, **16**, 834.
- [26] a) Cheng S, Rydberg A, Hjort K, *et al.* (2009) Liquid metal stretchable unbalanced loop antenna. *Appl. Phys. Lett.* **94** 144103 b) Cheng S, Wu Z G, Hallbjörner P, *et al.* (2009) Foldable and stretchable liquid metal planar inverted cone antenna. *IEEE Trans. Antennas Propag.* **57** 3765-3771; c) So JH, Thelen J, Qusba A, *et al.* (2010) Reversibly deformable and mechanically tunable fluidic antennas. *Adv. Funct. Mater.* **19** 3632-3637; d) Kubo M, Li X, Kim C, *et al.* (2010) Stretchable microfluidic radiofrequency antennas. *Adv. Mater.* **22** 2749-2752.
- [27] Cheng S, Wu Z. (2010) Microfluidic stretchable RF electronics. *Lab Chip* **10** 3227-323
- [28] Chiechi R C, Weiss E A, Dickey M D, *et al.* (2008) Eutectic gallium-indium (EGaIn): A moldable liquid metal for electrical characterization of self-assembled monolayers. *Angew. Chem. Int. Ed.* **47** 142-144
- [29] Koo H J, So J H, Dickey M D, *et al.* (2011) Towards all-soft matter circuits: Prototypes of quasi-liquid devices with memristor characteristics. *Adv. Mater.* **23** 3559-3564
- [30] Yang Y, Sun N, Cheng P, *et al.* (2018) Liquid-Metal-Based Super-Stretchable and Structure-Designable Triboelectric Nanogenerator for Wearable Electronics. *ACS Nano* **12** 2027-2034
- [31] Krupenkin T, Taylor J A. (2011) Reverse electrowetting as a new approach to high-power energy harvesting. *Nat. Commun.* **2** 448
- [32] Eaker C, Dickey M D. (2016) Liquid metal actuation by electrical control of interfacial tension. *Appl. Phys. Rev.* **3** 031103
- [33] Tang S Y, Khoshmanesh. K, Sivan V, Petersen P, *et al.* (2014) Liquid metal enabled pump. *PNAS* **3** 3304
- [34] Park Y L, Chen B R, Wood R J. (2012) Design and fabrication of soft artificial skin using embedded microchannels and liquid conductors. *IEEE Sensors* **12** 2711-2718
- [35] Palleau E, Reece S, Desai S C, *et al.* (2013) Self-healing stretchable wires for reconfigurable circuit wiring and 3D microfluidics. *Adv. Mater.* **25** 1589-1592

- [36] Boley J W, White E L, George T C, Chiu, Kramer R K. (2014) Direct Writing of Gallium-Indium Alloy for Stretchable Electronics. *Adv. Funct. Mater.* **24** 3501-3507
- [37] Zheng Y, He Z, Gao Y, Liu J. (2013) Direct Desktop Printed-Circuits-on-Paper Flexible Electronics. *Sci. Rep.* **3** 1786
- [38] Ladd C, So J H, Muth J, Dickey M D. (2013) 3D Printing of Free Standing Liquid Metal Microstructures. *Adv. Mater.* **25** 5081-5085
- [39] Zheng Y, Zhang Q, Liu J. (2013) Pervasive liquid metal based direct writing electronics with roller-ball pen. *Aip Adv.* **3** 112117
- [40] Li G, Wu X, Lee D W. (2016) A galinstan-based inkjet printing system for highly stretchable electronics with self-healing capability. *Lab Chip* **16** 1366
- [41] Boley J W, White E L, Kramer R K. (2015) Mechanically Sintered Gallium-Indium Nanoparticles. *Adv. Mater.* **27** 2355-2360
- [42] Dickey M D, Chiechi R C, Larsen R J, Weiss E A, Weitz D A, Whitesides G M. (2008) Eutectic Gallium-Indium (EGaIn): A Liquid Metal Alloy for the Formation of Stable Structures in Microchannels at Room Temperature, *Adv. Funct. Mater.* **18** 1097-1104
- [43] Kim H J, Son C, Ziaie B. (2008) A multiaxial stretchable interconnect using liquid-alloy-filled elastomeric microchannels. *Applied Physics Letters* **92** 011904
- [44] So J H, Dickey M D. (2011) Inherently aligned microfluidic electrodes composed of liquid metal. *Lab Chip* **11** 905-911
- [45] Zhao W, Bischof J L, Hutasoit J, Liu X, Fitzgibbons T C, Hayes J R, Sazio P J, Liu C, Jain J K, Badding J V, Chan M H W. (2015) Single-Fluxon Controlled Resistance Switching in Centimeter-Long Superconducting Gallium-Indium Eutectic Nanowires. *Nano Lett.* **15** 153-158
- [46] Lin Y, Gordon O, Khan M R, Vasquez N, Genzer J, Dickey M D. (2017) Vacuum filling of complex microchannels with liquid metal. *Lab Chip* DOI: 10.1039/c7lc00426e
- [47] Gozen B A, Tabatabai A, Ozdoganlar O B, Majidi C. (2014) High-Density Soft-Matter Electronics with Micron-Scale Line Width. *Adv. Mater.* **26** 5211-5216
- [48] Li G, Wu X, Lee D W. (2015) Selectively plated stretchable liquid metal wires for transparent electronics. *Sensors and Actuators B* **221** 1114-1119
- [49] Li G, Lee D W. (2017) An advanced selective liquid-metal plating technique for stretchable biosensor applications. *Lab Chip* **17** 3415
- [50] Jeong S H, Hagman A, Hjort K, Jobs M, Sundqvist J, Wu Z. (2012) Liquid alloy printing of microfluidic stretchable electronics. *Lab Chip* **12** 4657-4664
- [51] Kramer R K, Majidi C, Wood R J. (2013) Masked Deposition of Gallium-Indium Alloys for Liquid-Embedded Elastomer Conductors. *Adv. Funct. Mater.* **23** 5292-5296
- [52] Tabatabai A, Fassler A, Usiak C, Majidi C. (2013) Liquid-Phase Gallium-Indium Alloy Electronics with Microcontact Printing. *Langmuir* **29** 6194-6200
- [53] Jeong S H, Hjort K, Wu Z. (2014) Tape Transfer Printing of a Liquid Metal Alloy for Stretchable RF Electronics. *Sensors* **14** 16311
- [54] Jeong S H, Hjort K, Wu Z. (2015) Tape Transfer Atomization Patterning of Liquid Alloys for Microfluidic Stretchable Wireless Power Transfer. *Sci. Rep.* **5** 8419
- [55] Park C W, Moon Y G, Seong H, Jung S W, Oh J Y, Na B S, Park N M, Lee S S, Im S G, Koo J B. (2016) Photolithography-Based Patterning of Liquid Metal Interconnects for Monolithically Integrated Stretchable Circuits. *ACS Appl. Mater. Interfaces* **8** 15459-15465
- [56] Varga M, Ladd C, Ma S, Holbery J, Tröster G. (2017) On-skin liquid metal inertial sensor. *Lab Chip* **17** 3272

- [57] Lu T, Finkenauer L, Wissman J, Majidi C. (2014) Rapid Prototyping for Soft-Matter Electronics. *Adv. Funct. Mater.* DOI: 10.1002/adfm.201303732
- [58] Lu T, Markvicka E J, Yu J, Majidi C. (2017) Soft-Matter Printed Circuit Board with UV Laser Micropatterning. *ACS Appl. Mater. Interfaces* **9** 22055-22062
- [59] Pan C, Kumar K, Li J, Markvicka E J, Herman P R, Majidi C. (2018) Visually Imperceptible Liquid-Metal Circuits for Transparent, Stretchable Electronics with Direct Laser Writing. *Adv. Mater.* **30** 1706937
- [60] Kazem N, Hellebrekers T, Majidi C. (2017) Soft Multifunctional Composites and Emulsions with Liquid Metals. *Adv. Mater.* **29** 1605985
- [61] Hohman J N, Kim M, Wadsworth G A, Bednar H R, Jiang J, LeThai M A, Weiss P S. (2011) Directing Substrate Morphology via Self-Assembly: Ligand-Mediated Scission of Gallium-Indium Microspheres to the Nanoscale. *Nano Lett.* **11** 5104-5110
- [62] Lin Y, Cooper C, Wang M, Adams J J, Genzer J, Dickey M D. (2015) Handwritten, Soft Circuit Boards and Antennas Using Liquid Metal Nanoparticles. *small* **11** 6397-6403
- [63] Dickey M D, Chiechi R C, Larsen R J, Weiss E A, Weitz D A, Whitesides G M. (2008) Eutectic Gallium-Indium (EGaIn): A Liquid Metal Alloy for the Formation of Stable Structures in Microchannels at Room Temperature. *Adv. Funct. Mater.* **18** 1097-1104
- [64] Mohammed M G, Kramer R. (2017) All-Printed Flexible and Stretchable Electronics. *Adv. Mater.* 1604965
- [65] Markvicka E J, Bartlett M D, Huang X, Majidi C. (2018) An autonomously electrically self-healing liquid metal-elastomer composite for robust soft-matter robotics and electronics. *Nature Materials* **17** 618-624
- [66] Lin Y, Genzer J, Dickey M D. (2020) Attributes, Fabrication, and Applications of Gallium-Based Liquid Metal Particles. *Adv. Sci.* 2000192
- [67] Deng B, Cheng G J. (2019) Pulsed Laser Modulated Shock Transition from Liquid Metal Nanoparticles to Mechanically and Thermally Robust Solid-Liquid Patterns. *Adv. Mater.* **31** 1807811
- [68] Tang L, Shang J, Jiang X. (2021) Multilayered electronic transfer tattoo that can enable the crease amplification effect. *Sci. Adv.* **7** eabe3778
- [69] Uppal A, Ralphs M, Kong W, Hart M, Rykaczewski K, Wang R Y. (2020) Pressure-Activated Thermal Transport via Oxide Shell Rupture in Liquid Metal Capsule Beds. *ACS Appl. Mater. Interfaces*. **12** 2625-2633
- [70] Neumann T V, Facchine E G, Leonardo B, Khan S, Dickey M D. (2020) Direct write printing of a self-encapsulating liquid metal-silicone composite. *Soft Matter* **16** 6608-6618
- [71] Morley N B, Burris J, Cadwallader L C, Nornberg M D. (2008) GaInSn usage in the research laboratory. *Rev. Sci. Instrument* **79** 056107
- [72] Kim J H, Kim S, So J H, Kim K, Koo H J. (2018) Cytotoxicity of Gallium-Indium Liquid Metal in an Aqueous Environment. *ACS Appl. Mater. Interfaces* **10** 17448-17454
- [73] Liu T, Sen P, Kim C J. (2010) Characterization of Liquid-Metal Galinstan *IEEE* **560**
- [74] Liu T, Sen P, Kim C J. (2012) Characterization of Nontoxic Liquid-Metal Alloy Galinstan for Applications in Microdevices. *Journal of Microelectromechanical systems* **21** 443
- [75] Lu Y, Lin Y, Chen Z, Hu Q, Liu Y, Yu S, Gao W, Dickey M D, Gu Z. (2017) Enhanced Endosomal Escape by Light-Fueled Liquid-Metal Transformer. *Nano Lett.* **17** 2138-2145

- [76] Zhu P, Gao S, Lin H, Lu X, Yang B, Zhang L, Chen Y, Shi J. (2019) Inorganic Nanoshell-Stabilized Liquid Metal for Targeted Photonanomedicine in NIR-II Biowindow. *Nano Lett.* **19** 2128-2137
- [77] Tang X, Alavi S. (2011) Recent advances in starch, polyvinyl alcohol based polymer blends, nanocomposites and their biodegradability. *Carbohydrate Polymers* **85** 7-16
- [78] Maribel I. Baker, 1 Steven P. Walsh, 2 Zvi Schwartz, 1 Barbara D. Boyan (2012) A review of polyvinyl alcohol and its uses in cartilage and orthopedic applications. *Journal of Biomedical Materials Research B: Applied Biomaterials* **5** 1451
- [79] Yeo W H, Kim S Y, Lee J, Ameen A, Shi L, Li M, Wang S, Ma R, Jin S H, Kang Z, Huang Y, Rogers J A. (2013) Multifunctional Epidermal Electronics Printed Directly Onto the Skin. *Adv. Mater.* **25** 2773-2778
- [80] Jeong S H, Zhang S, Hjort K, Hilborn J, Wu Z G. (2016) PDMS-Based Elastomer Tuned Soft, Stretchable, and Sticky for Epidermal Electronics. *Adv. Mater.* **28** 5830-5836
- [81] a) Jacquemoud C, Bruyere-Garnier K, Coret M. (2007) Methodology to determine failure characteristics of planar soft tissues using a dynamic tensile test. *Journal of Biomechanics* **40** 468-475
b) Joodaki H, Panzer M B. (2018) Skin mechanical properties and modeling: A review. *Proc IMechE Part H: Jengineering in Medicine* 1-21
- [82] Zhao X M, Xia Y N, Qin D, Whitesides G M. (1997) Fabrication of Polymeric Microstructures with High Aspect Ratios Using Shrinkable Polystyrene Films. *Adv. Mater.* **9** 251-254
- [83] Grimes A, Breslauer D N, Long M, Pegan J, Lee L P, Khine M. (2008) Shrinky-Dink Microfluidics: Rapid Generation of Deep and Rounded- Patterns. *Lab Chip* **8** 170-172
- [84] Nguyen D, Taylor D, Qian K, Norouzi N, Rasmussen J, Botzet, S, Lehmann, M, Halverson K, Khine M. (2010) Better Shrinkage than Shrinky-Dinks. *Lab Chip* **10** 1623-1626.
- [85] Chen C S; Breslauer D N; Luna J I; Grimes A; Chin W C; Lee L P; Khine, M. (2008) Shrinky-Dink Microfluidics: 3D Polystyrene Chips. *Lab Chip* **8** 622-624.
- [86] Turova N Y, Turevskaya E P, Kessler V G, Yanovskaya M I. (2002) The chemistry of metal alkoxides. 245.
- [87] N. Ashgriz, Handbook of Atomization and Spraying, *Springer* 184.
- [88] Mundo C, Sommerfeld M, Tropea C. (1995) Droplet-wall collisions experimental studies of the deformation and breakup process. *Int. J. Multiphase Flow* **21** 151.
- [89] Pasandideh-Fard M, Qiao Y M, Chandra S, Mostagimi J. (1996) Capillary effects during droplet impact on a solid surface. *Phys. Fluids* **8** 650.
- [90] Zheng B, Lin Y, Zhou Y, Lavernia E J, (2009) Gas Atomization of Amorphous Aluminum: Part I. Thermal Behavior Calculations Metall. *Mater. Trans.* **40B** 768.
- [91] Chen J, Kim S M, Kwon J Y. (2016) A Systematic Analysis of Drosophila Regulatory Peptide Expression in Enteroendocrine Cells. *Mol. Cells* **39** 358.
- [92] Veenstra J A, Agricola H J, Sellami A. (2008) Regulatory peptides in fruit fly midgut. *Cell Tissue Res.* **334** 499.
- [93] Veenstra J A, Ida T. (2014) More Drosophila enteroendocrine peptides: Orckinin B and the CCHamides 1 and 2. *Cell Tissue Res.* **357** 607.

- [94] Guo X, Yin C, Yang F, Zhang Y, Huang H, Wang J, Deng B, Cai T, Rao Y, Xi R. (2019) The Cellular Diversity and Transcription Factor Code of Drosophila Enteroendocrine Cells. *Cell Rep.* **29** 4172.
- [95] Amcheslavsky A, Song W, Li Q, Nie Y, Bragatto I, Ferrandon D, Perrimon N. Ip Y T. (2014) Enteroendocrine cells support intestinal stem-cell-mediated homeostasis in Drosophila. *Cell Rep.* **9** 32.
- [96] LaJeunesse D R, Johnson B, Presnell J S, Catignas K K, Zapotoczn G. (2010) Peristalsis in the junction region of the Drosophila larval midgut is modulated by DH31 expressing enteroendocrine cells. *BMC Physio.* **10** 14.
- [97] Benguettat O, Jneid R, Soltys J, Loudhaief R, Brun-Barale A, Osman D, Gallet A. (2018) The DH31/CGRP enteroendocrine peptide triggers intestinal contractions favoring the elimination of opportunistic bacteria. *Plos Pathog.* **14** e1007279.
- [98] Song W, Veenstra J A, Perrimon N. (2014) Control of lipid metabolism by tachykinin in Drosophila. *Cell Rep.* **9** 40.
- [99] Kamareddine L, Robins W P, Berkey C D, Mekalanos J J, Watnick P I. (2018) The Drosophila Immune Deficiency Pathway Modulates Enteroendocrine Function and Host Metabolism. *Cell Metab.* **28** 449.
- [100] Ameku T, Yoshinari Y, Texada M J, Kondo S, Amezawa K, Yoshizaki G, Shimada-Niwa Y, Niwa R. (2018) Midgut-derived neuropeptide F controls germline stem cell proliferation in a mating-dependent manner. *Plos biol.* **16** e2005004.
- [101] Doe C Q, Chu-LaGraff Q, Wright D M, Scott M P.(1991) The prospero gene specifies cell fates in the Drosophila central nervous system. *Cell* **65** 451.
- [102] Vaessin H, Grell E, Wolff E, Bier E, Jan L Y, Jan Y N. (1991) prospero is expressed in neuronal precursors and encodes a nuclear protein that is involved in the control of axonal outgrowth in Drosophila. *Cell* **67** 941.
- [103] Spana E P, Doe C. Q. (1995) The prospero transcription factor is asymmetrically localized to the cell cortex during neuroblast mitosis in Drosophila. *Development* **121** 3187.
- [104] Jiang H, Edgar B A. (2012) Intestinal stem cell function in Drosophila and mice. *Curr. Opin. Genet. Dev.* **22** 354.
- [105] Zhang Y Z, Li Y Y. (2014) Inflammatory bowel disease: pathogenesis. *World J. Gastroenterol.* **20** 91.
- [106] Biteau B, Jasper H.(2014) Slit/Robo signaling regulates cell fate decisions in the intestinal stem cell lineage of Drosophila. *Cell Rep.* **7** 1867.
- [107] Zeng X, Hou S X. (2015) Enteroendocrine cells are generated from stem cells through a distinct progenitor in the adult Drosophila posterior midgut. *Development* **142** 644.
- [108] Beehler-Evans R, Micchelli C A. (2015) Generation of enteroendocrine cell diversity in midgut stem cell lineages. *Development* **142** 654.
- [109] Miguel-Aliaga I, Jasper .Lemaitre B. (2018) Anatomy and Physiology of the Digestive Tract of Drosophila melanogaster. *Genetics* **210** 357.
- [110] Bonfini A, Liu X, Buchon N. (2016) From pathogens to microbiota: How Drosophila intestinal stem cells react to gut microbes. *Dev. com. immunol.* **64** 22-38.
- [111] Guo Z, Lucchetta E, Rafel N, Ohlstein B. (2016) Maintenance of the Adult Drosophila Intestine: All Roads Lead to Homeostasis. *Curr. Opin. Genet. Dev.* **40** 81-86.
- [112] Dai X, Zhou E, Yang W, Zhang X, Zhang W, Rao Y. (2019) D-Serine made by serine racemase in Drosophila intestine plays a physiological role in sleep. *Nat. Commun.* **10** 1986.

Acta Universitatis Upsaliensis

*Digital Comprehensive Summaries of Uppsala Dissertations
from the Faculty of Science and Technology 2097*

Editor: The Dean of the Faculty of Science and Technology

A doctoral dissertation from the Faculty of Science and Technology, Uppsala University, is usually a summary of a number of papers. A few copies of the complete dissertation are kept at major Swedish research libraries, while the summary alone is distributed internationally through the series Digital Comprehensive Summaries of Uppsala Dissertations from the Faculty of Science and Technology. (Prior to January, 2005, the series was published under the title "Comprehensive Summaries of Uppsala Dissertations from the Faculty of Science and Technology".)

Distribution: publications.uu.se
urn:nbn:se:uu:diva-459339



ACTA
UNIVERSITATIS
UPSALIENSIS
UPPSALA
2021